Journal of the Geological Survey of Brazil

Integration of multisource data to support the identification of lateritic regolith in Eastern - Bahia, northeastern Brazil

Edgar Romeo Herrera de Figueiredo Iza[1*], Rodrigo Soares Vieira dos Santos[1], Basílio Elesbão da Cruz Filho[1],

1 Serviço Geológico do Brasil – CPRM, Avenida Ulysses Guimarães, 2862 Sussuarana – Centro Administrativo da Bahia Salvador - BA – Brazil, CEP: 41213-000

Abstract

This work used multi-source data integration techniques (gamma-spectrometry, magnetometry, SRTM-altimetry) to identify areas favorable for the occurrence of well-developed lateritic regolith in the eastern region of the state of Bahia. The variables observed to define target potential were the high eTh/K and eU/K ratios and altitudes (obtained from SRTM). Based on these parameters, Boolean and fuzzy logic were applied to produce favorability maps. The best results were obtained under the fuzzy model (γ = 0.7) with a hit accuracy in the areas for potential laterite occurrence of 97.4% and a kappa value of 0.5, consisting of 118 control points obtained through fieldwork. The cross-referencing of the fuzzy image (γ = 0.7) with the magnetometry, total gradient (ASA-Analytical Signal Amplitude) suggested the predominance of more felsic protoliths in the most favorable areas. The lateritic index [IL = (eTh*eU)/K^2)] was also applied, demonstrating good correlation with the areas determined by the Boolean and Fuzzy models. Mineralogical associations (clay minerals and/or iron oxides) of the target areas were estimated by the Crósta Technique in OLI/Landsat-8 images. The processing results were integrated in GIS environment, together with control points and data found in the bibliography (e.g. geological map, vertical electrical profile, drill-holes, occurrence of Fe and Al, lateritic crusts, geochemical anomalies). The observed correlation between the generated models and the direct data validates the effectiveness of the techniques used.

Article Information

Publication type: Research paper
Submitted: 10 May 2019
Accept: 3 December 2019
On line pub: 19 February 2020
Editor: E.L. Klein

Keywords:
Laterite,
Lateritic crust,
eTh/K,
eU/K,
geophysics,
SRTM

*Corresponding author
Edgar Iza
E-mail address:
edgar.iza@cprm.gov.br

1. Introduction

Lateritic regolith occurs mainly in regions within the intertropical belt (latitudes between 30º N and 30º S), where laterization processes are most effective due to high temperatures and rainfall (Freyssinet et al. 2005).

Studies conducted in Australia (e.g. Wilford 1992, 2012; Anand and Paine 2002) and Central Africa (e.g. Arhin and Nude 2009; Arhin et al. 2015) based on the synergy of gamma-spectrometric, altimetric and orbital imaging have reached good results in mapping regolith and predicting relevant information for mineral prospecting (e.g. prospection maps). Smith et al. (2000) pointed out that at least thirteen gold deposits were discovered in Australia between 1983 and 1994, through geochemical studies of lateritic profiles integrated with regolith mapping.

In Brazil, the study of lateritic regolith has concentrated mainly in the Amazon region due to the extensive regolith presence and economical exploitation of associated mineral deposits (e.g. Al, Mn, Fe, Ni, etc.). The main research on regolith using airborne-gamma spectrometry and altimetric data also focused on this region (e.g. Carrino et al. 2011a; Iza et al. 2016b; Herrera 2016; Herrera et al 2016; Albuquerque 2018; Iza et al. 2018). However, most of the work is concentrated mainly on the geochemical and mineralogical aspects of the regolith profiles, focusing in part on the exploration of mineral resources and secondarily on geophysical and geochronological features.

In Bahia, where tropical climate predominates, about 25% of the area is mapped as Cenozoic surface formations with ferruginous lateritic crusts, calcrete and related residual materials standing out (Souza et al. 2003). The mapping of these areas was guided by geomorphological aspects (planed surfaces) in altimetric radar images and aerial photographs (e.g. King 1956; Silva Filho et al. 1974; Pedreira et al. 1975).

Although in the last decade the state of Bahia has been explored by high resolution airborne geophysical surveys and

This work is licensed under a Creative Commons Attribution 4.0 Internacional License.

ISSN: 2595-1939
https://doi.org/10.29396/jgsb.2020.v3.n1.1
Open access at jgsb.cprm.gov.br

simultaneously free orbital images were made available (e.g. OLI/Landsat, altimetric), there are no records of descriptive analysis and/or studies that integrate multi-source data (altimetry, airborne geophysics and remote sensing) focused on the study of regolith/weathering. In addition, there are several mineral resources with components related to supergene processes, such as Al, Fe, Ni, Mn, among others.

In this context, the purpose of this work is to carry out a study that integrates multi-source data (airborne geophysics, altimetry and remote sensing) in the eastern portion of the state of Bahia, in order to provide inputs for the geological mapping of the region and contribute to the discrimination of lateritic regolith and laterites themselves. Among the specific objectives of this work, the following stand out: a) definition of potential areas for the presence of well-developed lateritic profiles, through the integration of multi-source data (airborne geophysics, remote sensing and altimetry) and map algebra methods (Boolean and Fuzzy) and b) inference, based on aeromagnetic data, of probable types of parental rocks from areas with potential for lateritic profiles (crusts and associated latosols).

2. Variables included in the study of lateritic regolith

The main variables included in the formation of the regolith are climate, relief, source rock, weather, fauna and flora. Their combination will result in the most diverse products that constitute regolith (Thomas 1974; Butt and Zeegers 1992; Costa 2007). Thus, we highlight the three areas of knowledge related to the formation of lateritic profiles: tectonism associated with the possibility or impossibility of formation/preservation of the profiles; climatic aspects, which in turn are related to the intensity and speed of the change, and the source rock that will play a decisive role in the geochemical evolution of the alteration profile and the response of the rock to the weathering process. In this work, emphasis was given to the aspects of weathering and source rock and, for that, airborne geophysics (gamma-spectrometry and magnetometry), altimetry, geology and remote sensing were used.

Airborne gamma spectrometry (K, eTh, eU) is widely used in geological mapping, regolith mapping, and mineral research because of its ability to differentiate radiometric signatures of different lithologies (e.g. McQueen and Craig 1995; Wilford et al. 1997; Minty 1997; Scott and Pain 2008; Carrino et al. 2009, 2011a; Minty 2011; Wilford 2012, 2013; Arhin et al. 2015; Herrera 2016; Boissieu et al. 2018; Iza et al. 2018; Albuquerque 2018).

The behavior of chemical elements in relation to supergene processes is variable and depends on several factors, such as time, pH, oxygenation, climate, among other conditions (Wedepohl 1969; Butt and Zeegers 1992; Costa 2007). In any case, there are general behavioral trends when considering the impacts of elements on the unaltered rock and their products (thick soils, lateritic crust, etc.). These materials are commonly found where there are severe conditions of chemical weathering (hot and humid), typical of tropical areas.

Generally, in a supergene environment, according to Wedepohl (1969), Minty (1997), Dickson and Scott (1997), Wilford et al. (1997), Wilford (2002), due to its high solubility, K concentration generally decreases with increasing intensity of weathering, tending to be leached from primary minerals (e.g. micas, K-feldspars) or absorbed into clay minerals. In a supergene environment K tends to be mobile, remaining immobile only under very oxidizing conditions and simultaneously with pH above 9.5 (Takeno 2005). U and Th are considered less mobile. When released from minerals by weathering U is more mobile under oxidizing conditions but precipitates under reducing conditions. Under the latter condition only in situations where the pH is <4 Uranium becomes mobile again. Dickson and Scott (1997) also state that the mobility of U can be modified by adsorption in clay minerals, colloids, iron oxides and hydroxides. In these last two cases, there is a strong relationship with the formation of the ferruginous lateritic crusts. Although it can become mobile in combination with organic matter in soil and groundwater, Th tends to concentrate in regolith through resistate minerals and iron oxides. According to the aforementioned authors, these behaviors are more evident in pedogenetic processes. Only when pH is below 3, Th become mobile (Takeno 2005).

Dickson and Scott (1997) also claim that calcrete, ferricrete, pisolites and gossans (products resulting from intense weathering) each have their own geochemical signature and show that in these materials the mean values of K are low and of the order of <0.6% (pisolites), and those of U and Th vary between 2 and 130 ppm, showing remarkable discrepancy of behavior of the respective chemical elements and therefore high ratios Th/K and U/K. Table 1 shows the results obtained by Dickson and Scott (1997) and Iza (2017).

TABLE 1 – Radioelements in regolith material. Average values in brackets, Modified from Dickson and Scott (1997).

	Nº of samples	K %	U ppm	Th ppm
Calcrete	26	0.0 – 1.0 (0.3)	0.6 - 2.4 (1.2)	0.7 - 7 (3.2)
Ferricrete	32	0.1 - 0.6 (0.4)	1.7 - 4.3 (2.7)	9 - 130 (24.0)
Pisolite	71	0.0 - 4.4 (0.6)	1.7 - 5.0 (3.0)	7 - 100 (43.0)
Gossan	19	0.0 - 1.1 (0.4)	1.4 – 19.0 (6.0)	0.2 - 50 (12.0)
Laterite*	35	0.0 – 1.1 (0.1)	1.6 – 11.3 (5.4)	6.9 - 57.1 (29.9)

*Geochemical data of lateritic crusts by Iza (2017)

Therefore Dauth (1997), Wilford et al. (1997), Carrino (2011a) and other authors consider that the ratios eTh/K and eU/K are useful in determining potential areas for occurrence of thick regolith, soils, ferricrete, etc.

Figure 1 highlights the modified lateritic profile by Anand and Butt (1988), Anand et al. (1989) and Eggleton (2001). It includes the aluminous horizon based on the proposal of mature profile by Costa (1991). Moreover, the figure shows the simplified general distribution of lateritic and inherited minerals in a complete profile, as well as the schematic metallogenic zoning along it, showing different examples of mineralization according to each horizon (Costa 2007). In the left part of the picture a color legend similar to the one presented in the lateritic index (LI) figures was inserted in order to highlight and correlate (roughly) the radiometric response patterns especially related to the eTh/K and eU/K ratios in respect to each horizon of the weathering profile.

On the other hand, magnetic data is commonly used to investigate geology based on Earth's magnetic field anomalies resulting from the magnetic properties of subsurface rocks (Kearey et al. 2002). In the literature there

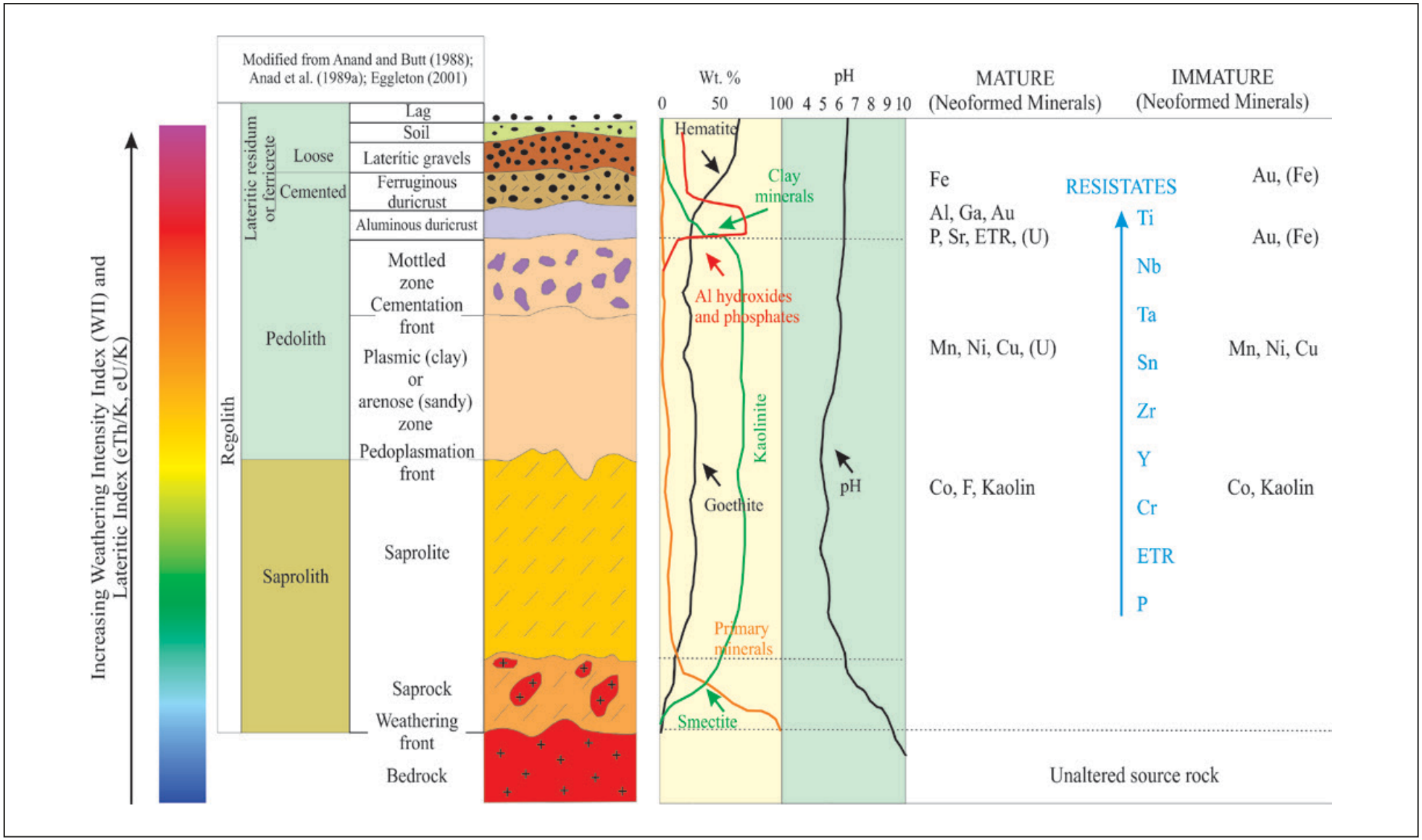

FIGURE 1 - Simplified general distribution of lateritic and inherited minerals in a complete lateritic profile and schematic metallogenic zoning along a lateritic profile, according to each horizon. Modified from Anand and Butt (1998), Anand et al. (1989) and Eggleton (2001) and Costa (2007).

are several references of airborne magnetometric data applications helping understand the distribution of the rock substrate magnetism thus contributing to the geological mapping itself (e.g. Batista et al. 2008; Carrino et al. 2011b). Magnetometry can, among other results, provide information about the boundary and shape of bodies, contribute to the delimitation of the main geological structures existing in a given area, as well as highlight the patterns of magnetic intensity of the rocky substrate.

Optical remote sensing makes it possible to map spectral reflectance of a thin surface layer, thus describing its mineral composition and providing information on the morphology of the terrain. OLI/Landsat satellite images are routinely used in regolith mapping (Craig et al., 1999). Spectral resolution of OLI/Landsat images distinguishes certain mineral groups. The Crósta technique, for example, enhances the response of clay minerals and iron oxides, and suppresses the effects of vegetation (Loughlin 1991).

Thus, the use of gamma-spectrometric ratios, relief data and remote sensing can contribute to delimiting potential areas for the occurrence of well-developed lateritic profiles (lateritic crusts and associated latosols). Based on the above assumptions, the various response patterns were analyzed to define the respective potential areas for the occurrence of well-developed lateritic profiles.

The theoretical basis used for the development and achievement of the objectives of this research was obtained from the works of An et al. (1991), Zimmermann (1985), Bonham-Carter (1994), Moreira et al. (2003), McBratney et al. (2003), Lagacherie (2005), Carranza (2009), Carrino et al. (2009, 2011a), Wilford (2012, 2013), Iza et al. (2016a) and Iza (2017).

3. Area location, climate, geomorphology and regional geological aspects

The research area of approximately 106,200 km^2, is located in the eastern state of Bahia (Figure 2A) and its main cities are: Ipirá, Feira de Santana, Itaberaba, Santo Antonio de Jesus, Valença, Jequié, Vitória da Conquista, Itabuna, Ilhéus and Itapetinga (Figure 2B). Altitudes range from 0 m on the east coast to 1501 m in the westernmost *Chapada Diamantina* region.

Mata Atlantica (Atlantic Forest) and Caatinga biomes are located in this region representing different physical (relief, climate, vegetation), economic, social and cultural characteristics. The first biome, located in the eastern region, has hot and humid climate, temperatures between 24 and 35ºC and rainfall between 1000 and 1500 mm per year. In the Caatinga region, located in the western part of the region, the climate is semi-arid, with average temperatures relatively similar to Mata Atlantica and annual average rainfall between 300 and 800 mm.

The geological context of the study area encompasses mainly the eastern portion of the San Francisco Craton (SFC), stabilized at the end of the Rhyacian Orogeny (~ 2.0 Ga), and part of the External and Internal Regions of the Araçuaí Fold Belt located south of the SFC formed during the Brasiliano Cycle (~ 600 Ma; Almeida 1981).

As Figure 2 shows, the basement of SFC corresponds to the most expressive unit of the area. It is compartmentalized into gneissic-migmatite crustal segments (3.2-2.6 Ga; Gavião Block to the west and Serrinha Block to the northeast), granulitic (2.8-2.3 Ga; Jequié Block in the central portion and Itabuna-Salvador-Curaçá), and gneissic (~ 2.7 Ga; Band Ipiae) crustal segments. Associated with these terranes occur Archean metavolcanic and sedimentary sequences and Paleoproterozoic metasedimentary sequences. These rocks are intruded by granitoids (granites, granodiorites and syenites), mafic and mafic-ultramafic bodies (mafic volcanics, gabbro, anorthosite, dunite, peridotite) with different dimensions and ages (Neoarchean to Paleoproterozoic). At the northwest end of the area the SFC platform cover is represented by Mesoproterozoic-Neoproterozoic clastic metasedimentary rocks (1.75-1.0 Ga; Espinhaço Supergroup) and Neoproterozoic clastic and carbonate rocks (1.00-700 Ma; San Francisco Supergroup). The Araçuaí Belt (AB) is formed by the Itapetinga Complex (amphibolite-facies orthogneisses, with supracrustal remnants) that corresponds to the part of the SFC basement that was intensely deformed during the Brasiliano Orogeny, besides intrusive Tonian anorogenic granitoids (Salto da Divisa Suite). In AB, near the southeast limits of the SFC, the Neoproterozoic metasedimentary rocks of the Rio Pardo (clastic sediments) and Macaúbas (clastic and carbonate sediments) groups and Caboclo Formation (clastic sediments) are found, in addition to granitic and alkaline intrusive rocks (Itabuna Intrusive Suite) of Neoproterozoic age. The Phanerozoic cover represented by Mesozoic sediments from the Recôncavo-Tucano and Camamú-Almada basins were deposited during the opening of the Atlantic Ocean, as well as the Cenozoic detrital and lateritic sediments from the Vitória da Conquista and Maracás plateaus, from the Atlantic coast and the alluvium.

4. Materials and methods

Figure 3 shows a summary of the materials used (airborne geophysics, digital elevation model (DEM), OLI / Landsat 8) and the main procedures performed.

4.1. Airborne geophysics

The study area is covered by three aero geophysical projects consisting of aeromagnetic and aero-gamma spectrometric profiles with flight lines spaced at 500 m. They are: the Ruy Barbosa - Vitória da Conquista (CPBM 2007); Cândido Sales - Mascote (CBPM 2009) and the Ipirá - Ilhéus Aero geophysical Project (CBPM and CPRM 2011), which together cover 100% of the area. More information can be found in the reports of the respective projects.

Geophysical data was treated using Oasis Montaj 9.2 (Geosoft) software. Initially, negative values were excluded from the aero-gamma spectrometric data. The gridding of the K, eTh and eU channels of the projects was performed using the Minimum Curvature interpolation method (Briggs 1974). As the data were acquired in surveys carried out under different conditions, the grids were compensated using the linear relationship between the overlapping area data between the different airborne surveys. Subsequently, compensated grids were integrated using the Oasis Montaj Grid Knitting menu to generate the mosaic of each radio element that encompasses the entire study area.

The individual channel grids of K, eTh, eU, eTh/K and eU/K ratios and total gradient (ASA-Analytical Signal Amplitude image) were transformed to GeoTIFF format by Geosoft extension in ArcGIS environment (ESRI).

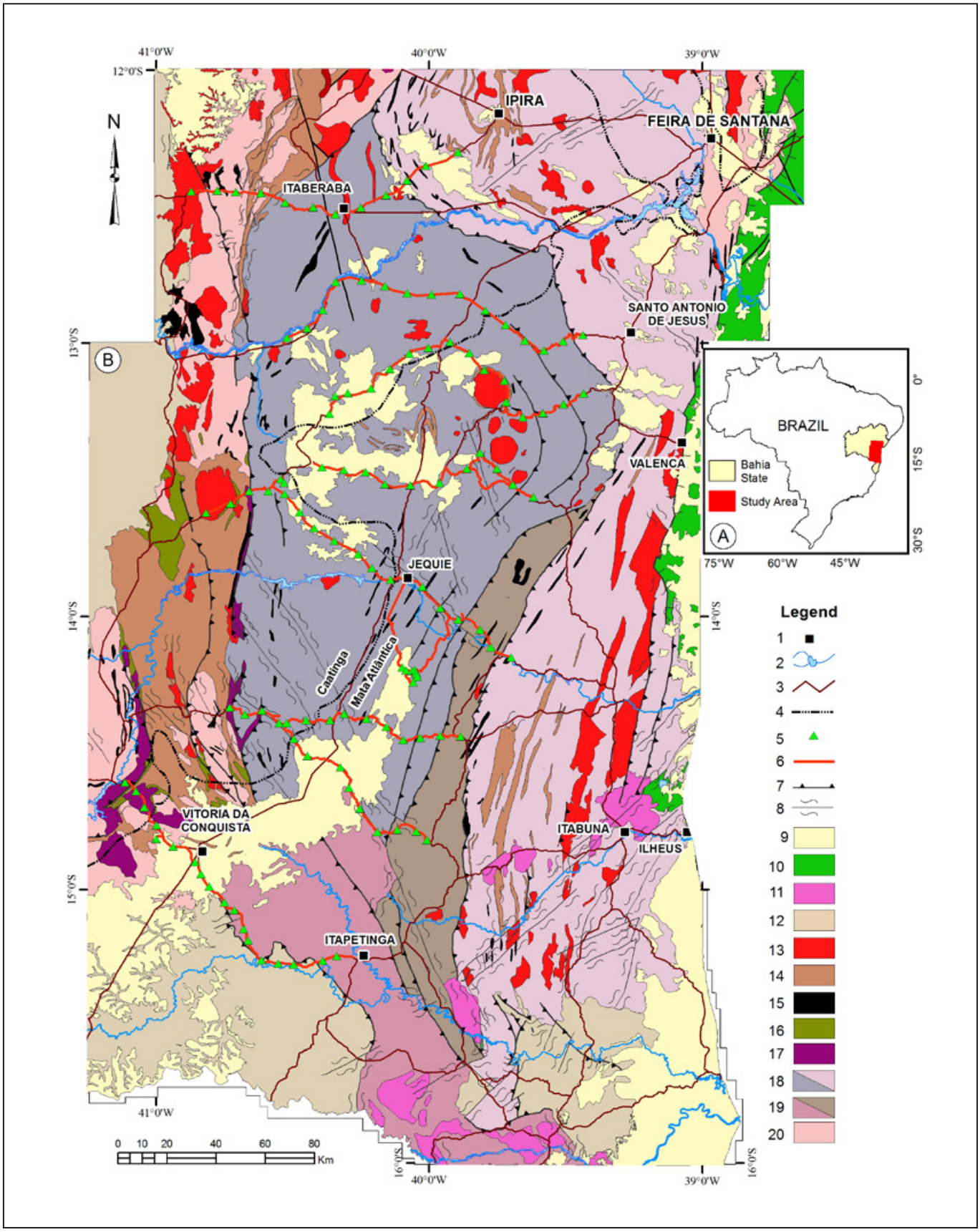

FIGURE 2 - A - Location of the study area; B- Simplified geological map of Souza et al. (2003). Caption: 1. Cities; 2. Rivers; 3. Roads; 4. Margins of the biomes; 5. Points visited; 6. Tracks; 7. Thrust faults; 8. Shear zones; 9.Cenozoic covers; 10. Mesozoic covers; 11. Neoarchean granitoids; 12. Mesoproterozoic-Neoproterozoic covers; 13. Paleoproterozoic granitoids; 14. Neoarchean to Paleoproterozoic metasedimentary sequences; 15. Archean and Paleoproterozoic mafic-ultramafic bodies; 16. Neoarchean metavolcanic-sedimentary sequences; 17. Neoarchean granitoids; 18. Granulite of the Itabuna-Salvador-Curaçá and Jequié blocks; 19. Gneisses of the Ipiaú Band and Itapetinga Complex; 20. Gneisses-migmatites of the Gavião (west) and Serrinha (east) blocks.

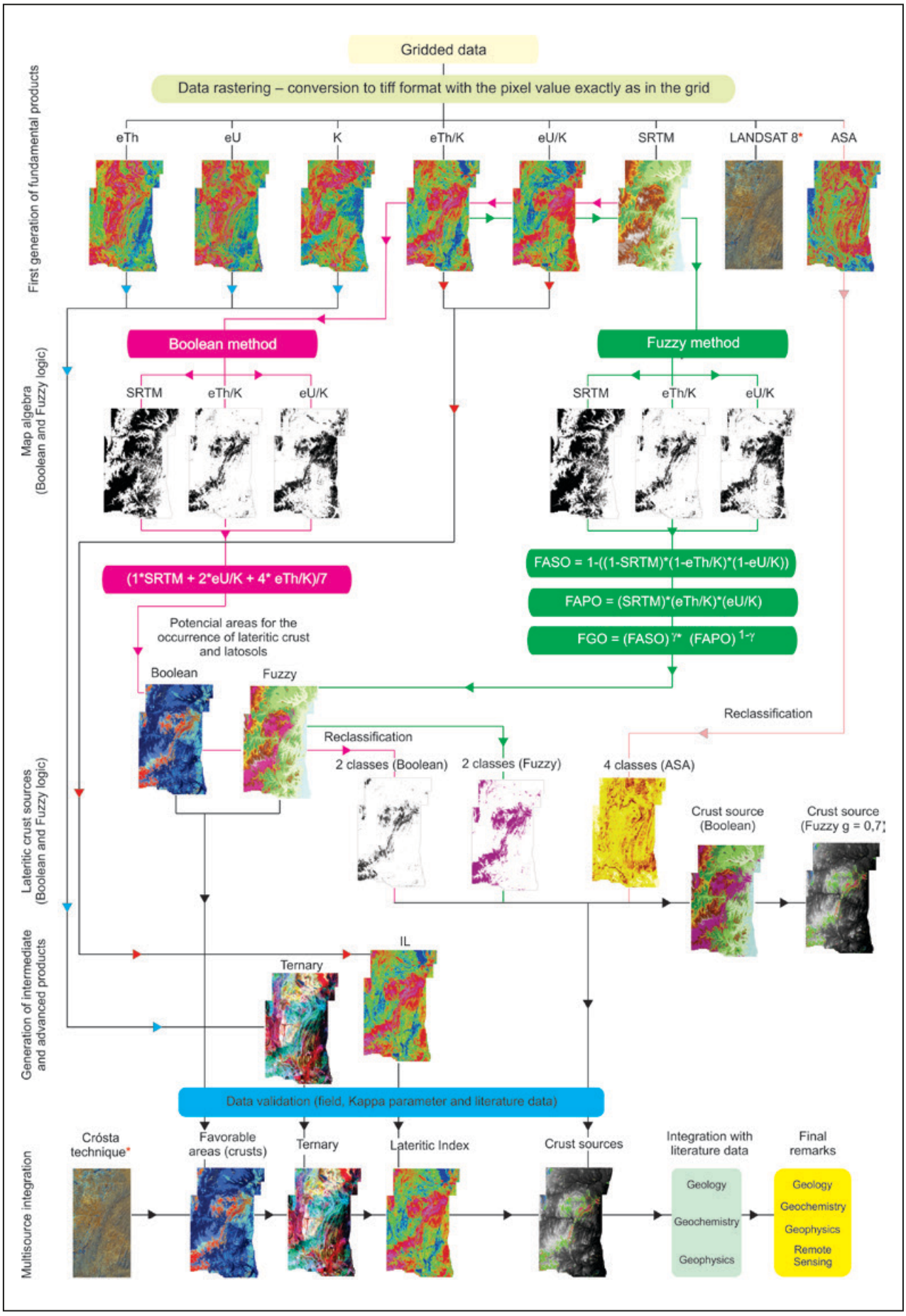

FIGURE 3 - Flowchart with the main procedures performed with the aero-geophysical data, SRTM DEM and respective products.

4.2. Shuttle Radar Topography Mission - SRTM

The NASA (2000) MDE data, with a spatial resolution of 90 meters, were used to define dimensions and the main intervals related to lateritic crust occurrences and respective relief forms.

4.3. Remote sensing

Remote sensing was used to confirm areas with presence of mineral paragenesis associated with the weathering process, such as kaolinite, hematite, goethite among other iron oxides and hydroxides. In this sense, in multispectral images (bands 2 to 7) of the Operational Land Imager (OLI) sensor aboard the Landsat 8 Satellite, the Crósta technique (or Feature Oriented Components Selection - FOCS) was applied with the help of ENVI software. The scenes with the orbit/points 216/69 and 216/70 imaged on 19/06/2017 were acquired from USGS (2019). This technique involves the analysis of the main components of two groups of four bands, considering the spectral responses of the mineral assemblies composed of iron oxides (OLI bands 2, 4, 5 and 6) and clay minerals (OLI bands 2, 5, 6 and 7). The principal components (PC) generated for each group allowed us to select the one that best enhances the material analyzed (reflectance and absorption signature). In the first group we chose the "iron" band (PC 4) and in the second the "clay" band. (PC 3). After the selection of the PCs, a color composition was made by allocating clay (Hy image) in red, sum of iron oxides and clay (Image Hy + Fe) in green and iron oxide in blue (image Fe).

4.4. Fieldwork

To confirm the data and to validate the models, a field stage was carried out, culminating in the execution of 8 longitudinal geological sections of approximate east-west direction (Figure 2), with an approximate total length of 1700 km. A total of 118 points were visited and the rocky outcrops and the regolith itself were described (soils, rust and alumina lateritic crusts, mottled horizon, saprolite, etc.).

Figure 2B details the accesses used to perform the fieldwork and respective points visited for data validation, a topic discussed in sections 4 and 5.

4.5. Mathematical models

4.5.1. Boolean Logic

The logic is based on a binary system, where "0" represents "false" and "1" represents "true". In the case of geological, pedological, geomorphological data, among others, the output maps need to be classified into appropriate count values for the mapping, i.e. they should provide a complete analysis of all variables and allow map visualization.

In this work, the input binary maps were generated from the gamma-spectrometric ratios (eTh/K, eU/K) and from the SRTM image altimetric data. The ratios were adopted to emphasize the discrepancies between the elements and consequently highlight the most favorable areas for the occurrence of lateritic crust and associated latosols and therefore the high intensity of weathering. According to the assumptions presented in sections 1 and 2, the median and absolute deviation of the median data were used to delimit the areas where lateritic crust is most likely to occur. However, in some cases the results were extremely restrictive and did not represent all the outcropping surface formations. Alternatively, the values greater than the average plus the standard deviation of the ratios eTh/K and eU/K were transformed to "1" and the lower values were transformed to "0", generating new reclassified images for both ratios. The SRTM data (altimetry) represented the current occurrence of mapped crusts and their respective altitudes. Thus, the value "1" was used for elevations between 200 and 300 m, and between 600 and 1501 m; and "0" for elevations between 0 and 200 m and between 300 and 600 m.

4.5.1.1. Index Overlay Method

Bonham-Carter (1994) added the Index Overlay Method (IOM) to the Boolean technique, which consists of attributing different weights to each input variable (map), considering the level of importance according to the hypothesis evaluated. In this aspect, the intention is to create maps with the widest possible spectrum of results, enabling the visualization of the areas of influence of each variable and/or their combinations (Bonham-Carter 1994; Carranza 2009). We emphasize that the weights are subjectively attributed, considering not only the importance of each variable, but the context of each case evaluated and the previous knowledge of the data analyst.

IOM is an enhanced version of the Boolean method as it allows to assign weights to input data and produce maps with values between 0 and 1 and not just 0 or 1. Thus each input image (eTh/K, eU/K and MDE SRTM) has a weight that depends on the hypothesis considered. Each map was multiplied by its corresponding weight and then summed to finally be normalized by the sum of the weights (Eq. 1). The result is a value between 0 and 1, which can be classified at appropriate mapping intervals (Bonham-Carter, 1994).

$$S = \frac{(1 * SRTM + 2 * eU/K + 4 * eTh/K)}{7} \qquad (Eq. 1)$$

Where: S is the score for each pixel of the final image; 7 is the sum of the weights.

Thus, each input map received a weight that belongs to a geometric progression with common ratio of 2. More weight was given to the gamma-spectrometry because the high eTh/K and eU/K ratios highlight well the areas with intense weathering. However, a lower weight was attributed to the eU/K ratio (when compared to the eTh/K ratio) due to the higher mobility of U when compared to the Th. The resulting final classes range from 0 to 1 and indicate areas with the lowest probability (0) and the highest probability (1) of lateritic crusts, latosols and their erosion products.

The resulting maps showed areas with higher (IOM classes ≥5) or lower (IOM classes <5) potential for the occurrence of well-developed lateritic profiles with lateritic crusts and associated latosols.

4.5.2. Fuzzy Method

The fuzzy method (Bonham-Carter 1994) initially considers the transformation of grid images to TIFF images with rescaled pixels between 0 and 1. The images chosen in the *fuzzy* process were eTh/K, eU/K, and SRTM DEM. The *membership large* was applied to the ratios in order to highlight the high values, that is, the areas with intense weathering. In

the SRTM/MDT image the data was maintained and neither the high nor low values were highlighted. In the next step, the images were submitted to the Fuzzy Algebraic Sum Operator (FASO) according to equation 2:

$$FASO = \left((1 - SRTM) * \left(1 - \frac{eTh}{K}\right) * \left(1 - \frac{eU}{K}\right)\right) \qquad (Eq.2)$$

In FASO, when any of the variables (SRTM, or eTh/K or eU/K) is too high, i.e. close to 1, the result for the final image pixel will tend to 1 regardless of the values of the other variables. The result in this case will be a less restrictive image and therefore with more potential areas for occurrence of lateritic crusts.

The Fuzzy Algebraic Product Operator (FAPO) was then applied according to equation 3:

$$FAPO = (SRTM) * \left(\frac{eTh}{K}\right) * \left(\frac{eU}{K}\right) \qquad (Eq.3)$$

In this stage the objective was, besides obtaining results based on distinct algebraic approaches, to provide an evaluation of the more or less optimistic preliminary results of the lateritic crust and latosol occurrence areas. In FAPO when any of the variables tend to 0 the pixel result in the final image will tend to 0 regardless of the value of the other variables. In other words, the final FAPO image is more restrictive than, for example, FASO and will therefore have fewer potential areas for lateritic crusting. In both cases, high values (favorable areas for the occurrence of crusts and latosols) were considered as above-average values plus standard deviation.

The final step of the fuzzy method considered the application of the fuzzy gamma operator (FGO) which tends to simultaneously rebalance the results obtained in FAPO and FASO, according to equation 4:

$$FGO = (FASO)^{\gamma} * (FAPO)^{1-\gamma} \qquad (Eq.4)$$

The γ values range from 0 to 1, and those close to 1 tend to emphasize the algebraic sum results while those closer to 0 tend to highlight those of the algebraic product. In the study area we chose to use γ = 0.3 and 0.7, which represent, respectively, the most pessimistic and optimistic results for the occurrence of lateritic crusts and associated latosols.

4.6. Definition of laterite crust sources

In the later stage, the objective was to superimpose the favorable areas obtained in the Boolean logic (favorable areas - classes IOM 5 to 7, Table 2) and Fuzzy logic (gamma 0.7, Table 3) with the total gradient data (ASA). The idea was to evaluate the subsurface magnetic intensity and thus estimate the type of protolith associated with lateritic crust and latosols. The result obtained by the Boolean method (final image IOM) was transformed into a binary image 0 and 1. The values converted to 1 were those with classes IOM ≥ 5 and the values converted to 0 were those with classes IOM <5. The total gradient image was reclassified into 4 classes according to the mean and standard deviation of the data. In general terms, there is a tendency for higher magnetic intensity in mafic rocks and lower in felsic rocks. Thus, the classes (magnetic intensity ranges) were named as: very high, high, low and very low. The end result of the intersection between gamma spectrometry and magnetometry (map algebra) was the crust source map that simultaneously highlights the potential areas for the occurrence of well-developed lateritic profiles with lateritic crusts, latosols and their erosion products (gamma spectrometry), as well as the respective magnetic intensity of their substrate (magnetometry).

4.7. Lateritic Index

To compare the results of potential areas for the occurrence of thick regolith obtained in this research (Boolean, fuzzy technique, etc.), the lateritic index (LI) was also used. This index was developed to further analyze the relationship between weathering and gamma-spectrometric data (Iza 2018).

The lateritic index (LI) is calculated considering exclusively the relation of impoverishment of K and enrichment of Th and U during the weathering process. In this index, it is considered the product between the ratios eTh/K and eU/K that result in equation 5:

$$LI = \frac{(eTh * eU)}{K^2} \qquad (Eq.5)$$

Where: LI is the lateritic index; eTh is the thorium channel; eU is the uranium channel and K refers to the potassium channel.

The LI allows to distinguish areas with different degrees of weathering (greater or lesser probabilities of laterization) and / or truncation of lateritic profile. Areas with high LI suggest a higher potential for more developed and/or complete lateritic profiles, that is, with presence of lateritic crusts and associated latosols, while areas with low lateritic index are more likely to represent rock, saprolite and subordinate less developed lateritic profiles (Figure 1).

4.8. Kappa coefficient of agreement

The kappa coefficient (κ) (confusion matrix) was used to determine the agreement between the Boolean and Fuzzy models and the field observations. The considered variables comprised: 1) outcrops with rock and saprolite, or subordinately, soils with undeveloped “B” horizon (e.g. neosols, cambisols), considered low maturity group (lateritic profile poorly developed); 2) well-developed “B” horizon soils (latosols, etc.), more than 2 meters thick, and/or ferruginous/alumina lateritic crusts, a group considered to be of high maturity.

From the analysis of these variables, each point observed in the field was classified as “not expected within the model” (Group 1) or “expected within the model” (Group 2). Subsequently, the kappa coefficient was calculated for each model (Boolean and fuzzy), comparing the field data with the areas indicated as high potential for the occurrence of a well-developed lateritic profile. The 118 points were analyzed and compared with the models generating 4 classes that feed the calculation of the referred coefficient.

Class 1 (true positive) occurs when the field point is “expected within the model” and, after confrontation, it appears that it is, in fact, within the area calculated as high potential for occurrence of well-developed lateritic profile, representing a model fit. Class 2 (true negative) occurs when the field point is “not expected within the model” and, after analysis, it appears that it is indeed outside the area calculated as high potential for occurrence of well-developed lateritic profile, a model fit. Class

3 (false positive) is the situation where the field point is "not expected within the model" and, after evaluation, it is found to be within the calculated area of high potential for a well-developed lateritic profile occurrence, representing a model error. Class 4 (false negative) occurs when the field point is "expected within the model" and, after confrontation, it is observed that it is outside the area calculated as high potential for the occurrence of a well-developed lateritic profile, representing a model error.

The coefficient κ is defined by equation 6:

$$k = \frac{n\sum_{i=1}^{c} x_{ii} - \sum_{i=1}^{c} x_{i+}x_{+i}}{n^2 - \sum_{i=1}^{c} x_{i+}x_{+i}} \qquad (Eq.6)$$

Where x_{ii} is the value in row I and column I, x_i + is the sum of row i; $x_{+\ i}$ is the sum of column i of the confusion matrix, n is the total number of samples, and c is the number of classes (Cohen 1960).

According to Landis and Koch (1977), the kappa value between 0.81 and 1 is considered as perfect correlation. Kappa between 0.61 and 0.8 has a substantial correlation while the values between 0.60 and 0.41 have a moderate correlation, between 0.4 and 0.21 considerable, 0.20 to 0 slight and poor when close to 0. In the present work, the kappa coefficient for each model was calculated by means of an order 2 confusion matrix that is represented by the numbers obtained in the 4 above classes.

Results

5.1. Boolean Model Analysis (index overlay)

The application of the Boolean model (index overlay method - IOM), allowed to obtain 8 favorability classes for the occurrence of latosols, lateritic crusts and products of their disaggregation (well-developed lateritic profile). These classes are the result of the absence of variables until the combination (sum) of all of them. The domains classified as favorable represent about 8.9% of the studied area, constituting approximately 9500 km^2, and have influence at least of the ratio eTh/K + SRTM (weights 5 to 7 and classes IOM = 0.71 to 1), as shown in table 2.

These results are relatively similar to those observed by Herrera 2016 and Iza et al. (2016a, 2016b) who, using the same technique in the southwestern portion of the Brazilian Amazon, determined the occurrence of lateritic crusts and their breakdown products at 6.6% and 7.84%, respectively. Figure 4 shows the Boolean result (combination of all IOM variables-weights) and the respective areas considered favorable (weights ≥5) and unfavorable (weights <5).

5.2. Fuzzy Model Analysis

The application of the fuzzy method considered the use of the algebraic sum (FASO), the algebraic product (FAPO) and finally the use of the fuzzy gamma operator (FGO). The favorability domains highlighted by FASO and FAPO are reasonably similar to the results of Boolean logic. However, the areas highlighted by FASO are slightly more continuous, especially in the northwest and south and identified 22.2% of the area as favorable for lateritic crust and latosols (Table 3). Other areas with lower expression, not observed in the Boolean method, are also individualized in the northern and southern portions. These results are largely associated with greater control of the values of the variables included in the Boolean method when compared to the Fuzzy method.

The result of the algebraic product (FAPO) indicates 11.4% of the area as favorable for the occurrence of lateritic crusts and associated latosols (table 3). Unlike the algebraic sum,

Table 2. Classes defined by IOM for the study area.

Weight (Σ)	Classe IOM	Variable	Area Km²	Accumulated Area	Area %	Accumulated Area %	Classes
0	0	None	47,296.92	47,296.92	44.5	44.5	Unfavorable
1	0.14	SRTM	33,488.78	80,785.70	31.5	76.0	Unfavorable
2	0.29	U/K	8,897.70	89,683.40	8.4	84.4	Unfavorable
3	0.43	SRTM + U/K	6,687.89	96,371.29	6.3	90.7	Unfavorable
4	0.57	Th/K	366.15	96,737.45	0.3	91.1	Unfavorable
5	0.71	Th/K + SRTM	767.51	97,504.96	0.7	91.8	Favorable
6	0.86	Th/K + U/K	2,101.51	99,606.48	2.0	93.8	Favorable
7	1	Th/K + U/K + SRTM	6,636.10	106,242.59	6.2	100.0	Very favorable

Table 3. Classes defined by fuzzy method (FASO, FAPO and FGO of 0.3 and 0.7) for the study area.

Operator	Classes fuzzy	Area Km²	Accumulated Area	Area %	Accumulated Area %	Classes
FASO	0.000 - 0.710	82,635.531	82.635,53	77.8	77.8	Unfavorable
	0.710 – 1.000	23,533.875	106,169.406	22.2	100.0	Favorable
FAPO	0.000 - 0.087	94,033.797	94.033,797	88.6	88.6	Unfavorable
	0.087 - 0.516	12,135.609	106,169.406	11.4	100.0	Favorable
FGO (g= 0.3)	0.000 - 0.144	92,149.531	87.090,922	86.8	86.8	Unfavorable
	0.144 - 0.629	140,19.875	106,169.406	13.2	100.0	Favorable
FGO (g =0.7)	0.000 - 0.303	87,090.922	87,090.922	82.0	82.0	Unfavorable
	0.303 - 0.818	19,078.484	106,169.406	18.0	100.0	Favorable

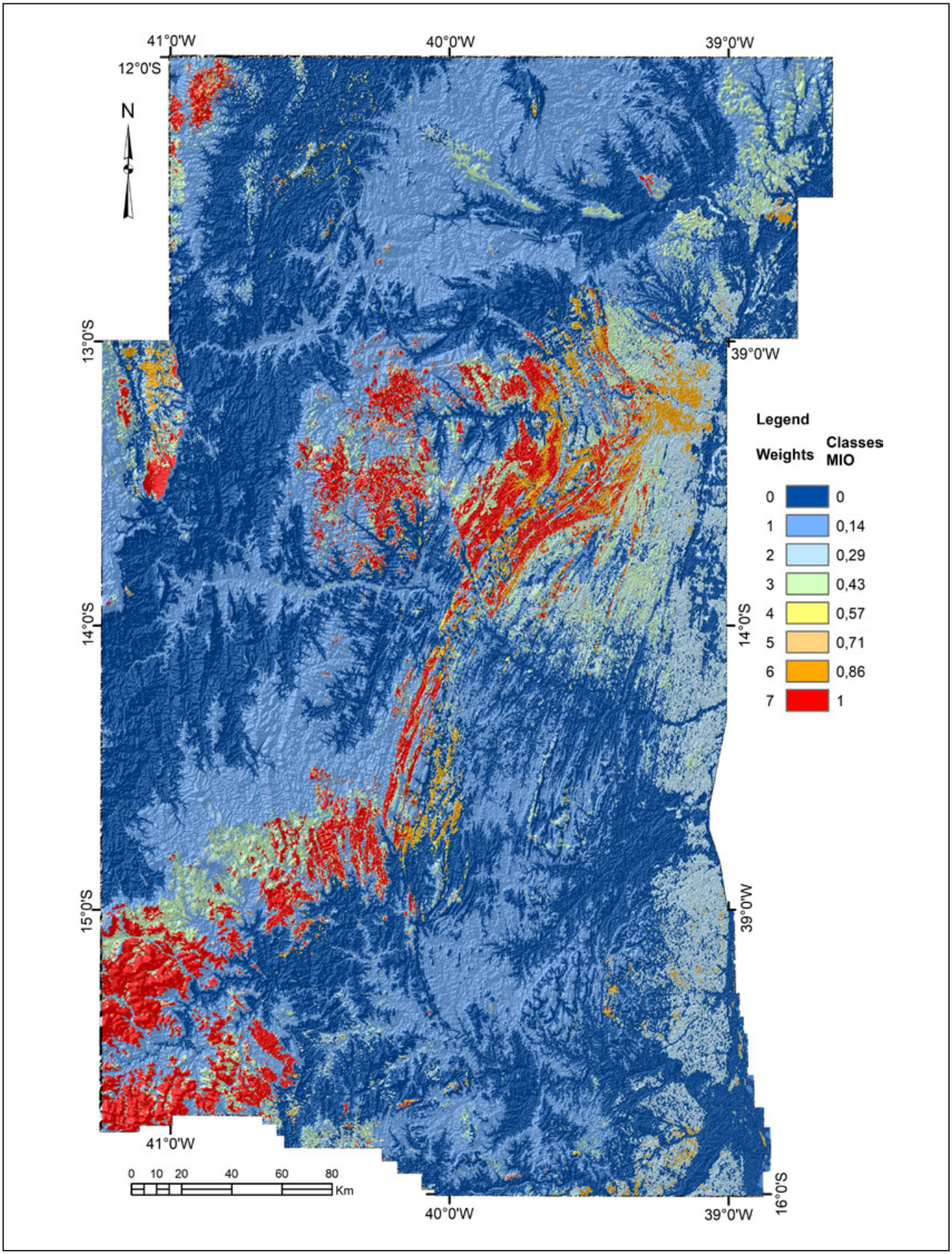

FIGURE 4 - Map of potential areas for the occurrence of well-developed lateritic profiles with presence of lateritic crusts, lat osols by the Boolean method (MIO), highlighting the 8 classes of predictability. Classes 5, 6 and 7 are considered to have high potential for the occurrence of lateritic crusts and associated latosols (well-developed lateritic profiles).

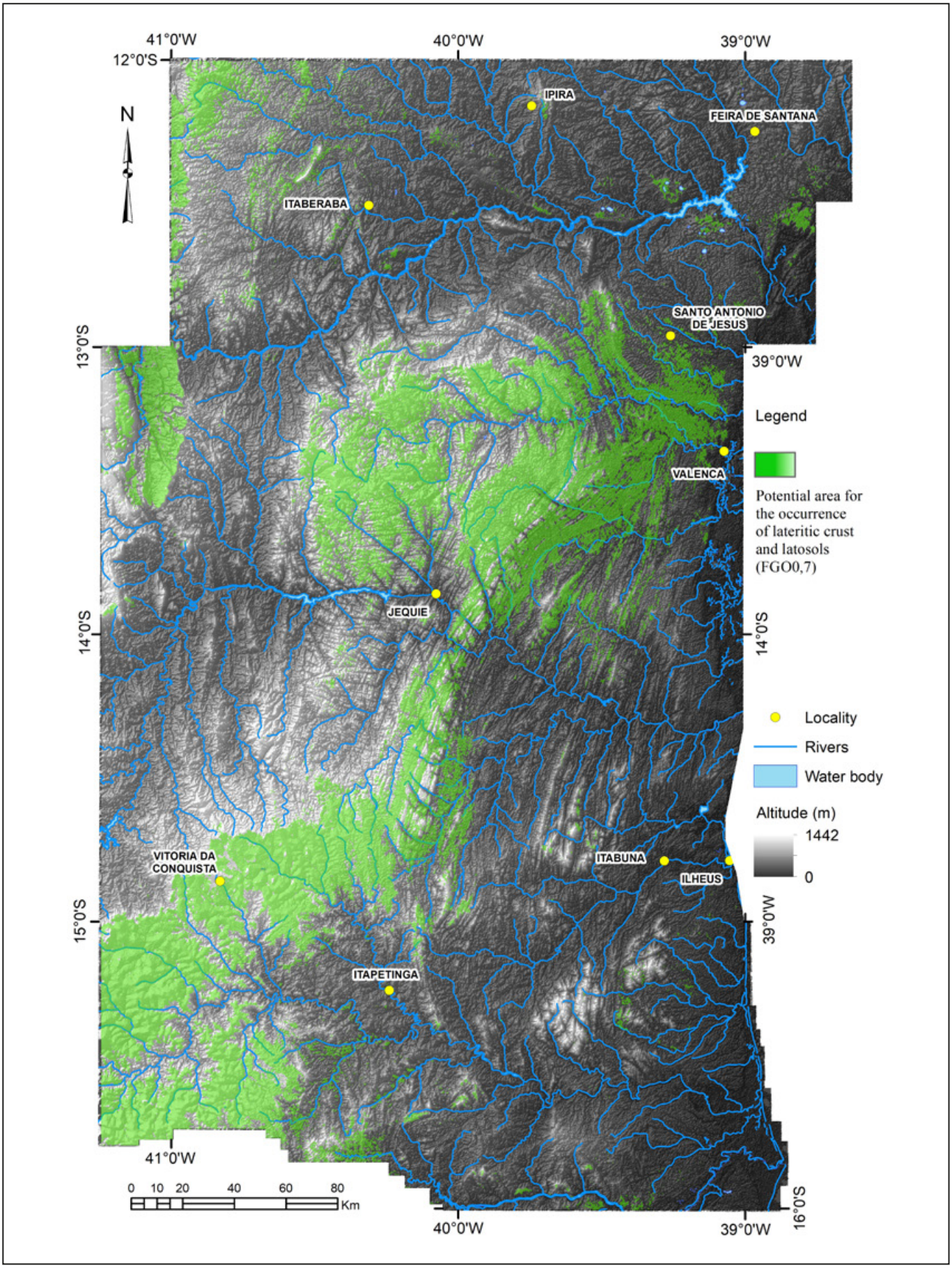

FIGURE 5 - Map of potential areas for the occurrence of well-developed lateritic profiles with lateritic crusts, latosols and their erosion products by the fuzzy method (fuzzy gamma operator (γ = 0.7) superimposed on the SRTM / MDT).

the FAPO restricts the areas, especially those located below 500 m altitude. In this context, the potential areas existing in FASO and located in the north and south-southeast portion are not highlighted by the algebraic product. In the final step of the fuzzy model, the fuzzy gamma operator (FGO) was applied with the value γ = 0.3 and 0.7. The main characteristic of the operator is to balance the results obtained in FASO and FAPO. In this paper the results of FAPO and FGO of 0.3 are similar exactly because the smaller values of γ (<0.3) tend to result in results similar to FAPO, however, the latter subtly highlights additional areas, for example in the northeast portion of the area. Figure 5 represents the most optimistic result for the occurrence of lateritic crusts and associated latosols (FGO 0.7), which delimits about 18% of the area with high potential.

5.3 Model Validation

The Boolean model indicated the most pessimistic result among the 3 models, with the area calculated as favorable representing 8.9% of the total area, which is reflected in the kappa coefficient of agreement of 0.14. Of the 118 points collected, only 13 are within the calculated favorable region, with the other points located outside. Regarding the points within the area, the model mapped efficiently, hitting 12 of the 13 points as favorable for the occurrence of well-developed lateritic profile (92.3% accuracy). The Boolean model, as it is more pessimistic, did not show the same efficiency in the points outside the favorable area, hitting 50 of the 105 points as being unfavorable (47.6% right). Although it was efficient in mapping the favorable points, the pessimistic character and the much higher number of points outside the model generated a high number of false negatives that were determinant for the low kappa value.

The Fuzzy gamma 0.3 model also proved to be a pessimistic model, although it is less restrictive than the Boolean model, classifying about 13.2% of the total area as favorable area for the occurrence of well-developed lateritic profile, and deriving kappa coefficient of 0.45 (moderate correlation). It appeared that the Fuzzy gamma 0.3 model was also efficient in mapping the favorable points, hitting 34 of the 35 points that are located within the delimited area as favorable (97.2% correct). Of the points located outside the favorable area, the model hit 50 out of 83 points (60.2% hit).

The fuzzy 0.7 gamma model is the most optimistic of the three models studied. Like the other two, it was effective in mapping points located within the calculated area as favorable, hitting 37 of the 38 expected points within the model (97.4% accuracy). Of the 80 points outside the favorable region, it hit 50 as unexpected within the model (62.5% hit). The kappa coefficient of the fuzzy model 0.7 is 0.5 (moderate correlation) (Table 4).

TABLE 4 – Matrixes of confusion and kappa coefficients for Boolean and Fuzzy.

Forecast	Boolean	Fuzzy γ 0.3	Fuzzy γ 0.7
True positive	12	34	37
True negative	50	50	50
False positive	1	1	1
False negative	55	33	30
Coefficient Kappa (κ)	0.14	0.45	0.50

In general, the models proved to be able to map the areas most favorable for the occurrence of well-developed lateritic profiles, since they all hit more than 90% of the points within the calculated favorable areas. It is worth adding that all points where aluminum or ferruginous crust were observed are located within the areas calculated by the models.

5.4 Lateritic regolith protolith (Latosols and lateritic crusts)

The ASA image was divided into four classes of magnetism intensity considering especially the mean and standard deviation. The comparison between magnetic data (ASA-total gradient) and gamma-spectrometry (potential areas for lateritic crust) allowed us to suggest the probable parental rocks of the lateritic crust. In this sense, the potential area for lateritic crusts and latosols predicted by the Boolean method overlaps with protoliths with low to very low magnetic intensity in 82% of the forecast area, while 18% is overlapping with high to very high magnetic intensity protoliths, while the integration between the fuzzy model (gamma 0.7) and the ASA image shows overlapping potential areas for lateritic crust with low to very low magnetic intensity protoliths in 84% of the forecast area, and 16% overlaps with high to very high magnetic intensity protoliths (Figure 6).

These results indicate the dominance of less magnetic (biased towards felsic) source rocks, which provides evidence on the prevalence and / or potential of any geochemical associations and consequently on the metallogenetic potential of the lateritic profile.

5.5. Lateritic Index

The lateritic index application considered the eTh/K and eU/K ratios in order to highlight the different levels of weathering in the study area (Figure 7). High LI domains represent about 9% of the total area and substantially restrict potential areas for lateritic regolith occurrence. In any case, fieldwork contributed not only for validating the Boolean and Fuzzy models but also to provide a broader understanding of the weathering process itself in the field of study. In this work the areas delimited by the Boolean method are similar to those with high LI. Figures 8 and 9 describe field-verified rock outcrops and regolith in addition to their gamma-spectrometric (LI) standards.

6. Data integration and correlation with literature results

From the areas defined with high lateritic index, 3 target subareas were evaluated in order to compare the result with spectral, geochemical and mineral resources analyses.

6.1 Subarea 1

Subarea 1 is the central domain of the project area, where the major mineral occurrences (e.g. Al, Ni, Mn and Fe) and the highest relative LI values occur (Figure 10). In this domain, there are also occurrences of lateritic crusts recorded in the field stage of this project, as well as in data obtained by Fernandes (1995), Martins and Santos (1997), Santos (2010) and Alves (2018).

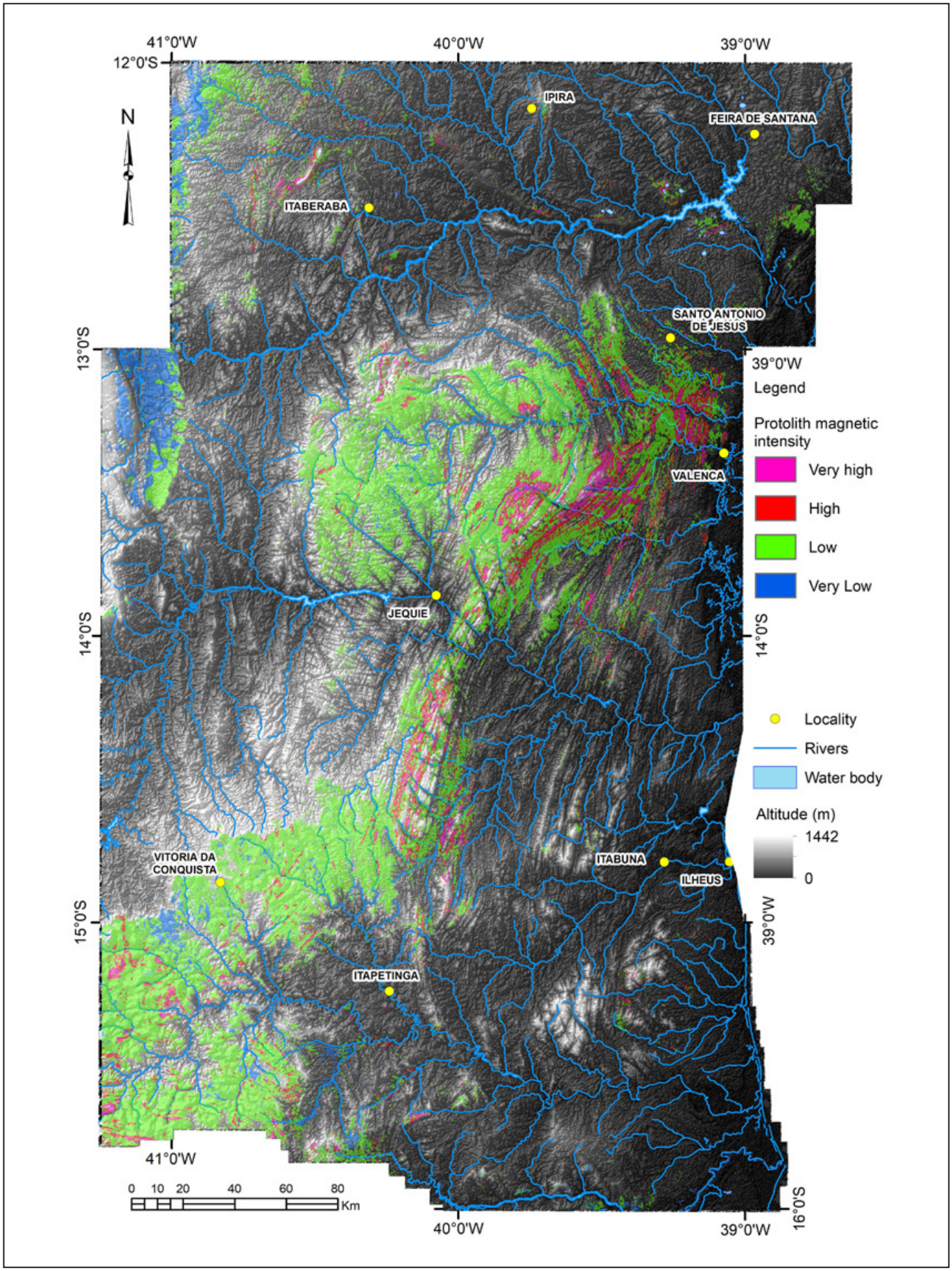

FIGURE 6 - Map of potential areas for the occurrence of well-developed lateritic profiles with presence of lateritic crust by the fuzzy method (FGO 0.7) superimposed on the SRTM MDE and respective protolith magnetic intensities (total gradient - ASA).

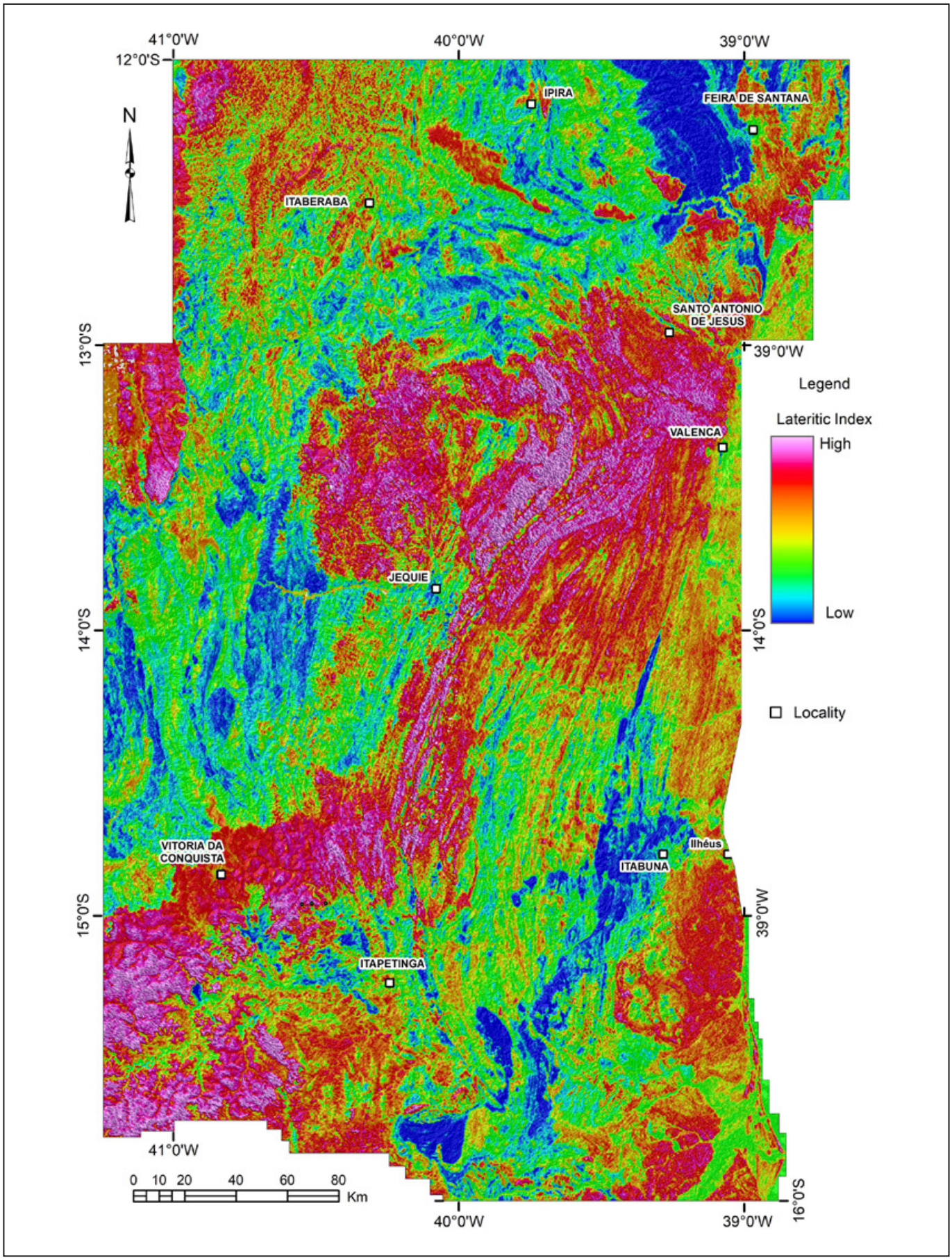

FIGURE 7 -Map of the lateritic index, highlighting in red and dark pink the areas with high index and therefore with high potential for occurrence of lateritic crust and associated latosols.

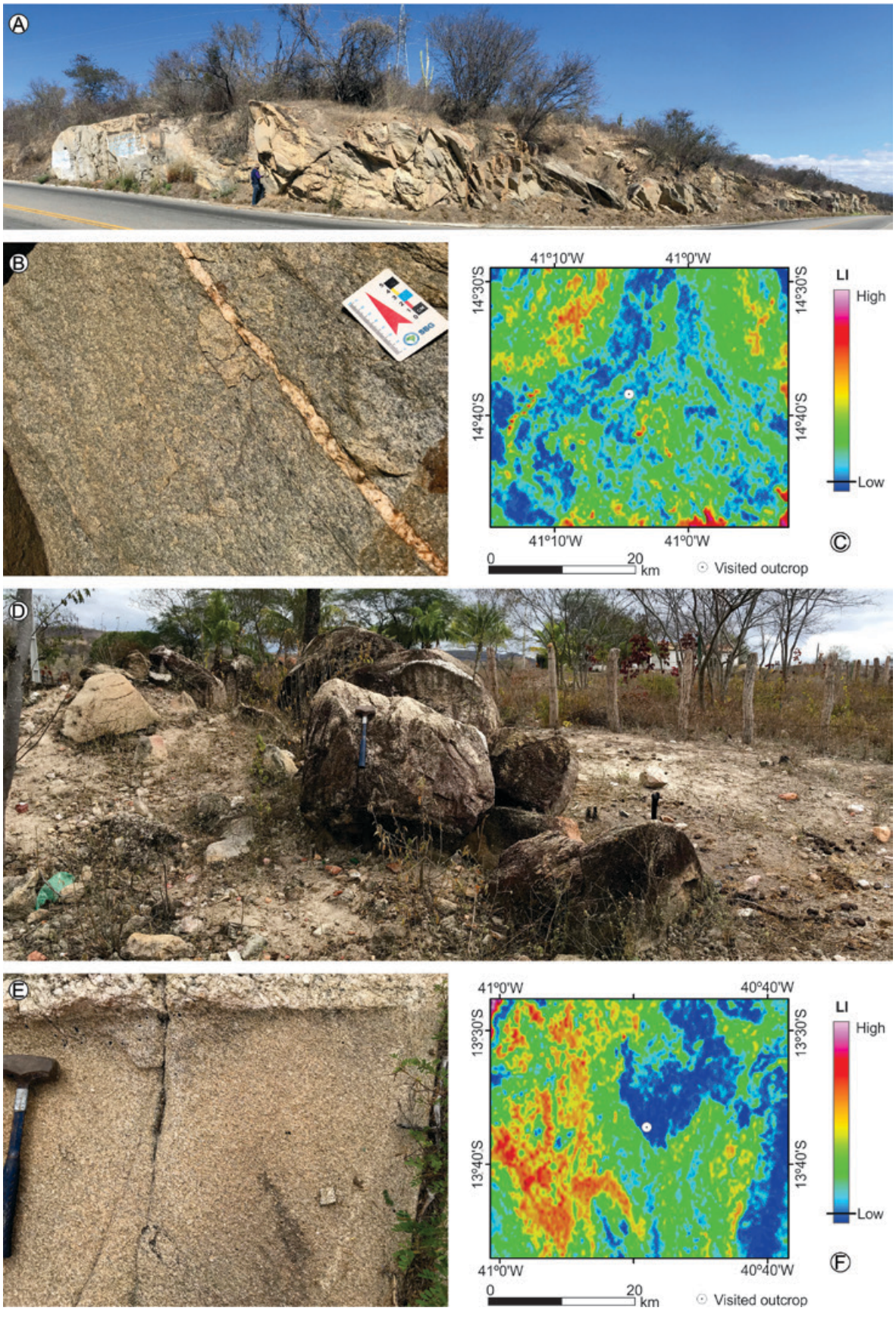

FIGURE 8 -Example of rock outcrop dominance. A) General appearance of granodiorite. B) Detail of the rock texture. C) Gamma-Spectrometric Context (LI). D) General view of the granite of the Iramaia and Contendas-Mirante region. E) Detail of the texture of the granite. F) Gamma-Spectrometric context (LI).

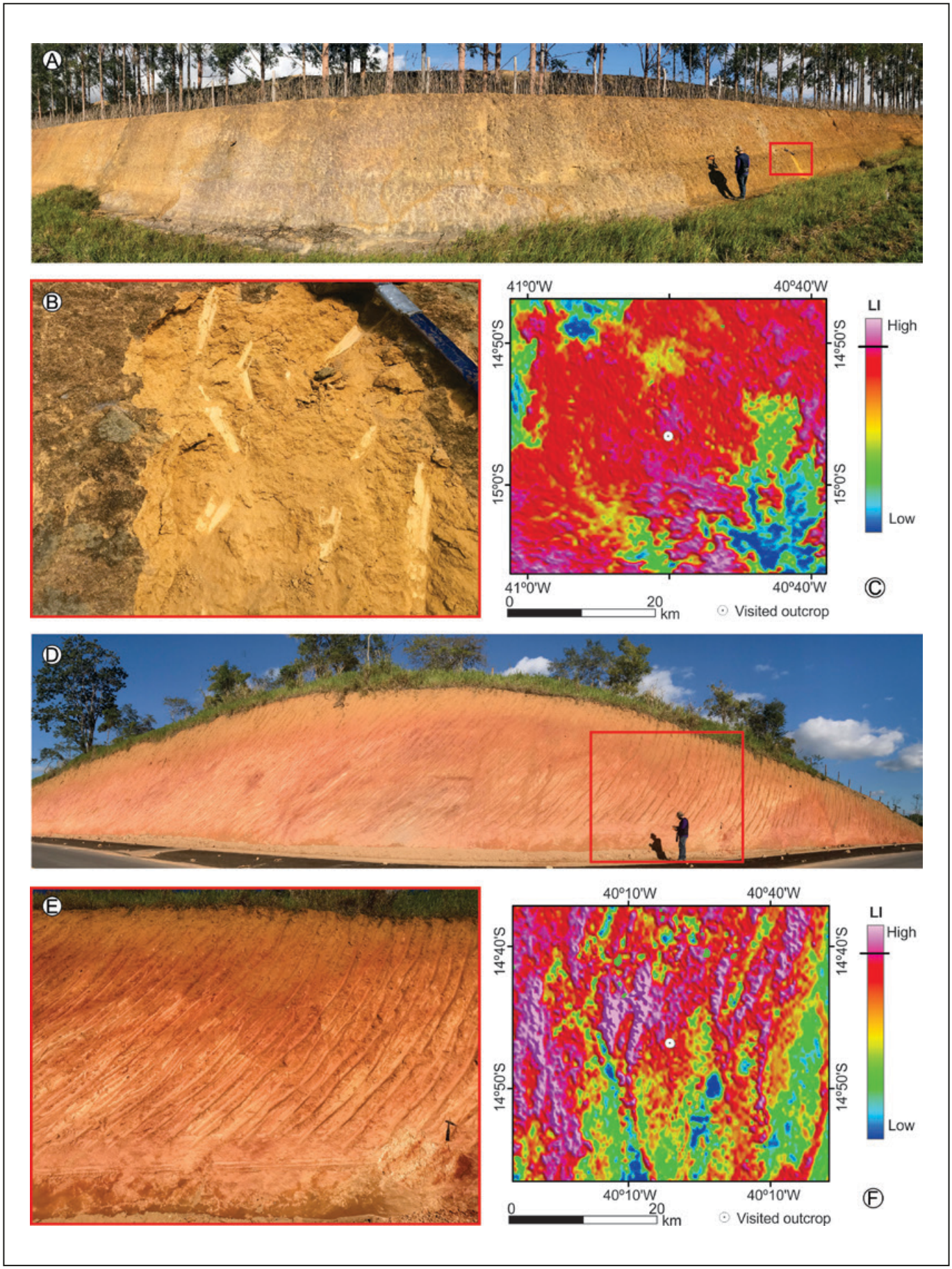

FIGURE 9 - Example of very thick soil dominance without rock or saprolite. A and D) General appearance of yellow clay soil with well-developed "B" horizon. B and E) Detail of the yellow soil. C and F) Gamma-Spectrometric Context (LI).

There is a strong correlation of known mineral occurrences (Al, Ni, Mn, Fe) with the highest lateritic index, especially Fe and Al, which occur predominantly in the central domain of subarea 1. With the exception of Al, the other mineral resources may be strongly linked to primary occurrences and/or intermediate horizons of the alteration profile (e.g. saprolite, pale zone, etc.) but most of them have a supergene component proven by fieldwork and several authors.

Fernandes (1995), addressing the Rare Earth Elements in Bahia, evaluated the economic potential of an area located in the southern region of this state, entirely included in the subarea 1 (Fig. 10). Among the results obtained stand out several radiometric anomalies (Ubaíra-Nova Canaã) with values between 350 and 15000 cps; in addition to anomalous geochemical associations in current sediment such as Cu-Ni-Cr; Fe-Co-Mn-V; Mg-Ba-Ni-Cr, Ca-Ba-Sr-Mg; and isolated anomalies, such as V, W, Nb, Co, Cu, among others.

Radiometric anomalies are, according to Fernandes (1995), strongly associated with Th and linked to hornblende leucogranites and allanite leucogranites, and lateritic soils developed on previous lithologies. The overlap between the LI-derived result and the radiometric results obtained by Fernandes (1995) are highly compatible. The high LI values indicate the domains with high eTh / K and eU / K ratios, and exactly in these regions the radiometric results obtained by the author exceed 15000 cps (Amargosa Fault domains, northeastern portion of subarea 1).

The geochemical associations show, for example, that variables linked to alkaline and alkaline earth metal elements correlate with low lateritic indicators (associations 7, 8 and partially 9) (Figure 10). On the other hand, associations with the presence of Cu-Ni-Cr, Fe-Co-Mn-V (associations 1, 2, 3, 4, 5, 6, 10, 11, 13 and 14), for example, show good correlation with areas of high lateritic index which confirms the efficiency of the index.

Martins and Santos (1997), observed the occurrence of several geochemical anomalies, including Cr-V, Mn-Ni-Co and Mn, related to the Almadina Complex, as well as V-Au anomalies in the Ibicuí Complex, and Nb-Ba associated with the Itabuna Intrusive Suite. In the anomalous area IVA and B (Figure 10, area 16), alkaline rocks (nepheline syenites) occur spatially associated with stream sediment anomalies and pan concentrate for Nb, Ba and Mn, and with gamma-spectrometric anomalies.

Within the limits of Ibicaraí sheet (southeastern portion of the study area) the metalotects responsible for the mineralization of Mn are aluminous gneisses (kinzigites) of the Almandina Complex (Martins and Santos 1997). The probable gondite levels of kinzigites that underwent supergene enrichment would have generated secondary concentrations of economic interest with over 5000 ppm Mn (Martins and Santos 1997). In the domains of the Ibicaraí sheet there are 16 Mn deposits, the main one located in the municipality of Coaraci (Figure 10). Other anomalous areas, evidenced by stream sediment data, highlight associations with the presence of Mn, such as those of number 14, 17, 19 (Figure 10). Both the anomalous areas and the occurrences present a certain level of correlation with the areas with high LI, indicating that this is a good prospective prognosis for the above mineral asset.

Santos (2010) described the Jiquiriçá River Basin Upper Aquifer (Maracás sheet 1: 100,000 - northwestern portion of subarea 1) and among other results described the geo-electrical aspects (electrical resistivity - vertical electrical sounding) of the geological units and of aquifers.

Among the main results, Santos (2010), highlighted regolith thicknesses ranging from 9 to 50 m. These results (regolith thickness > 10 m) were validated with well data and confirmed here by high LI values, which indicates the presence of well-developed lateritic profiles in the same region (Figure 10).

Alves (2018) characterized the litho-geochemistry of the laterite nickel proto-mineral of the Calembe region, and Lajedo do Tabocal identifying the in situ regolith thickness in 20 and 40 m boreholes, a result that is consistent with the high values of LI (Figure 10). Alves (2018) also shows that the Calembe ultramafic rocks present high Ni contents (1695 to 2601ppm) and the lateritic nickel proto-mineral is the serpentinite and serpentinized metadunites.

In turn, the ultramafic body of Fazenda Mirabela (nickel sulfide), located in the municipality of Itajibá hosts the Serra Azul nickel deposit. According to Silva and Sampaio (2017), mineralization related to: lateritic soils - clay minerals and iron oxides (oxidized ore); and with a lower horizon that is represented by green garnierite clays and ultramafic rock saprolite (silicate ore). In this case, there is also a good correlation of the Serra Azul Ni deposit area with areas of high LI (Figure 10).

From the results derived from the Crósta Technique applied to OLI sensor images related to Hy-HyFe-Fe (RGB) images, it is possible to highlight domains with spectral patterns compatible with the presence of iron, correlated with high IL (Figure 11). Emphasis is given to the south-northeast oriented central strip where occurrences of Fe, Al and lateritic crust have a high correlation with the presence of iron enhanced in blue colors in the composition of the images (Hy-HyFe-Fe, RGB).

The geological context (Figure 2) of the southwest-northwest domain highlighted in Figure 11 is essentially linked to enderbite, to charnoenderbite, and hornblende enderbite, as well as quartz-feldspar gneisses and supracrustal remnants, all interspersed with supracrustal rocks and mafic ultramafic bodies, largely belonging to the Jequié Complex and subordinate to the undifferentiated ultramafic mafic complex.

6.2 Subarea 2

Subarea 2 is located east of the city of Vitória da Conquista, on the edge of the Vitória da Conquista and Poções sheets (1: 100,000). In this area were highlighted six occurrences of iron, three of ferruginous lateritic crusts, and one of manganese, associated with high LI values.

In this subarea the lateritic crusts are immature and consist mainly of hematite, goethite and secondarily by kaolinite and quartz with rare associated gibbsite. In general, the exposures of the top of the lateritic profile show the presence of crusts up to 4 m thick, sometimes with columnar structure and vermiform texture. The crust is invariably covered by a dismantled horizon consisting of fragments of the lateritic crust itself dispersed in clayey sandy material. Against this horizon there is a dark gray to black organic soil level with average thicknesses of 30 cm (Figure 12 A and B). Field data associated with gamma-spectrometry (lateritic index) as well as those derived from the application of the Crósta technique reinforce this assertion by highlighting domains with high IL and simultaneous presence of Fe and hydroxyl-bearing minerals in the region (Figure 13A and B).

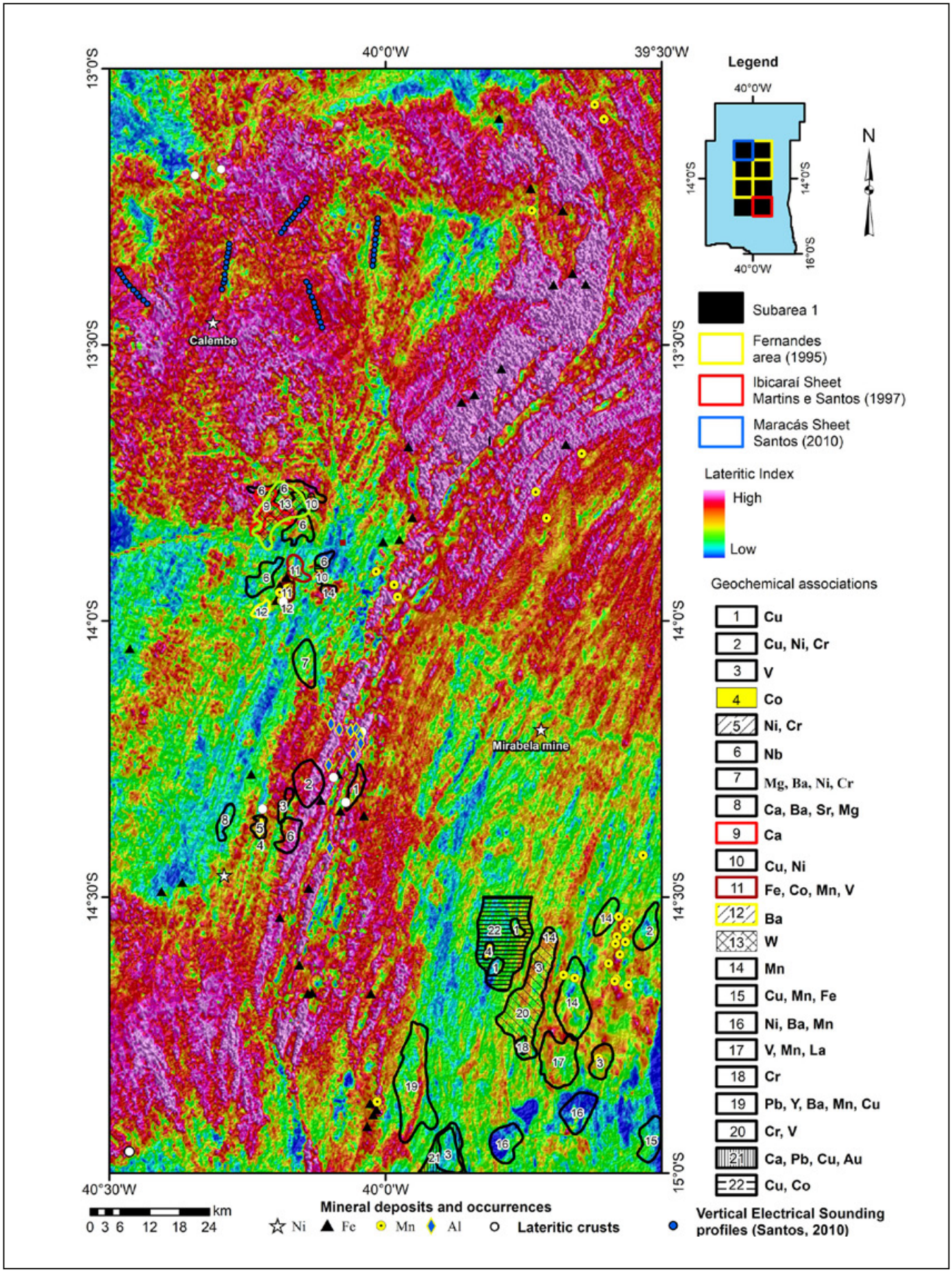

FIGURE 10 - Radiometric and geochemical data from Fernandes (1995) (Rare Earth Project Area), CPRM mineral resources (GeoSGB) and Electrical Vertical Sounding points by Santos (2010) overlapping with the lateritic index.

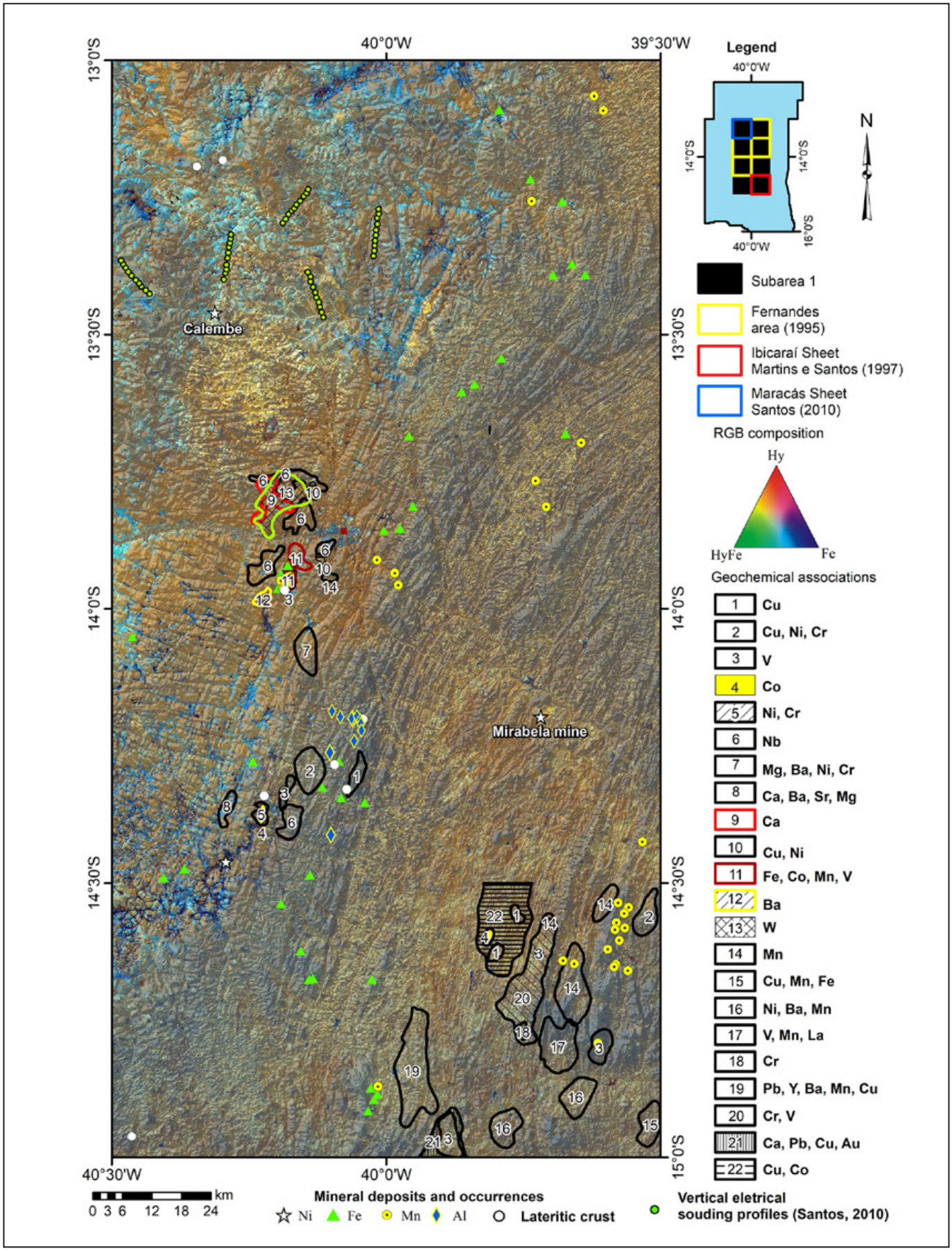

FIGURE 11 - Result of Hy (R), - Hy + Fe (G), - Fe (B) color composition derived from the Crósta technique on OLI/Landsat sensor images 8. Geochemical data from Fernandes (1995) (Area Terras Raras Project), mineral resources of the Geological Survey of Brazil data base (GeoSGB), and Electrical Vertical Sounding points (Santos 2010) are also shown.

6.3 Subarea 3

Subarea 3 is located in between the municipalities of Jequié and Itagi (north central portion of the area). In this domain, in addition to other mineral resources, there are dozens of aluminous lateritic crust points, nine of which were visited, as well as one occurrence of Fe. In the latter case, it is mainly an intensely weathered iron formation with a marked presence of magnetite, hematite and quartz and subordinate goethite.

Aluminous crusts occur on the tops of hills where a rolling relief with concave ridges prevails with colluviums sometimes found on the slopes. In this subarea there were no continuous flat surfaces, plains, plateaus or even small plateaus associated with the crusts. The crust is of red, pink to off-white hues, is massive and is invariably associated with clay soil of equally red, pink to off-white hues (Figure 14). At the top of the crusts a dismantled horizon at least 1-meter thick and consisting of centimeter size angular fragments is common. Outcrops can be up to 3 to 4 meters thick and have reasonable lateral continuity. In the valleys, the crusts, if they occur, form colluviums. In these areas altered rock outcrops probably comprising charnoenderbite (granulites from the Itabuna-Salvador-Curaçá and Jequié blocks) are rare.

Aluminous crust occurrences correlate with the high LI domains (Figures 10 and 15). Therefore, future investigations in the north and south domains should consider detailed studies in the medium to high LI domains, especially those related to Al, Fe, Mn, among others of supergene occurrence. Al and Fe occurrences also correlate with domains marked by iron-rich minerals (Figures 14 and 15).

7. Final remarks

The results obtained by integrating multi-source data (gamma-spectrometry, magnetometry and altimetry) correlate well with the geological units mapped as detrital-lateritic and undifferentiated covers (1.1.000.000 scale). These results confirm the potential of the techniques used. However, areas mapped as undifferentiated charnoenderbite and granulite of the Jequié Complex, Ibicui-Ipiaú orthogneisses, Caraíba Complex enderbite, and Ibicarai Complex enderbite have partial overlap with areas defined as having high potential for lateritic crust and latosols. In the field, however, there is a wide occurrence of ferruginous and alumina lateritic profiles in these same domains. These observations suggest the need for more detailed mappings and/or a more reliable representation of lateritic crust/lateritic profile in geological maps.

The products generated using the Boolean and Fuzzy methods proved to be robust tools for the mapping of regolith and mineral resources that may be related to the supergene enrichment process in eastern Bahia state.

The methods used identified between 8.9% and 18.0% (fuzzy range 0.7) of the study area as favorable for the occurrence of lateritic profiles, and, in addition, contributed to corroborate the results obtained with the use of LI. Using this methodological proposal, it was possible to sectorize areas of interest for future studies related to the elaboration of prospectivity maps for Al, Fe, Mn, Ni, among other metals related to lateritic profiles.

The use of magnetic data (total gradient - ASA) served as a complementary tool in understanding the weathering process as it suggests the level of magnetism of the parental rocks of the lateritic crust. The results show potential for associations not only linked to felsic rocks, but mafic/ultramafic rocks as well. This is supported by the Cu-Ni-Cr; Fe-Co-Mn-V; and Mg-Ba-Ni-Cr geochemical associations that indicate the presence of mafic/ultramafic source rocks in the region. Costa (2007), for example, considering the geochemistry of lateritic crust, states that high Cr, Mn, Ni, Co values combined with low REE, Sc, Y, Zr, Nb, Ta, Rb, Th are indicative of lateritic formations derived from mafic rocks, and high concentrations of Zr, Y, Sc, Nb, Ta, REE and Th show strong affinities with alkaline rocks.

The advantage of using LI is the speed of obtaining results, since there is no need for integration with relief data and map algebra, which is a decisive step in the elaboration of the Boolean and Fuzzy models. In any case, the high LI values generally show a good correlation with the results obtained with the Boolean and Fuzzy methods.

Remote sensing data, using the Crósta technique, allowed us to highlight not only areas with spectral patterns compatible with the predominance of Fe and hydroxyl-bearing minerals, but also the comparison of these results with those derived via gamma-spectrometric (LI) data integration.

FIGURE 12 - A) Example of lateritic crust with columnar structure about 1 m high. B) Detail of the hematite-rich rust crust.

In general, the integration of multi-source data proved to be robust in delimiting potential areas for lateritic crusting and associated latosols. The products presented here, such as the correlation map between the lateritic index and the total gradient (ASA), and the lateritic index map can be found respectively in Iza et al. (2019a, 2019b).

It is important to highlight that in the study area, there are several mineral occurrences and mines linked to Al, Fe, Mn, Ni, among other elements that are largely correlated to the supergene (or supergene component) enrichment processes. The regional records of Fe and Al occurrences are related to the presence of immature and mature lateritic profiles as well, that is, with the aluminum horizon (bauxitic and/or phosphate) according to the classification of Costa (1991). Therefore, the area of study has good mineral potential and is therefore of relevant regional mineral

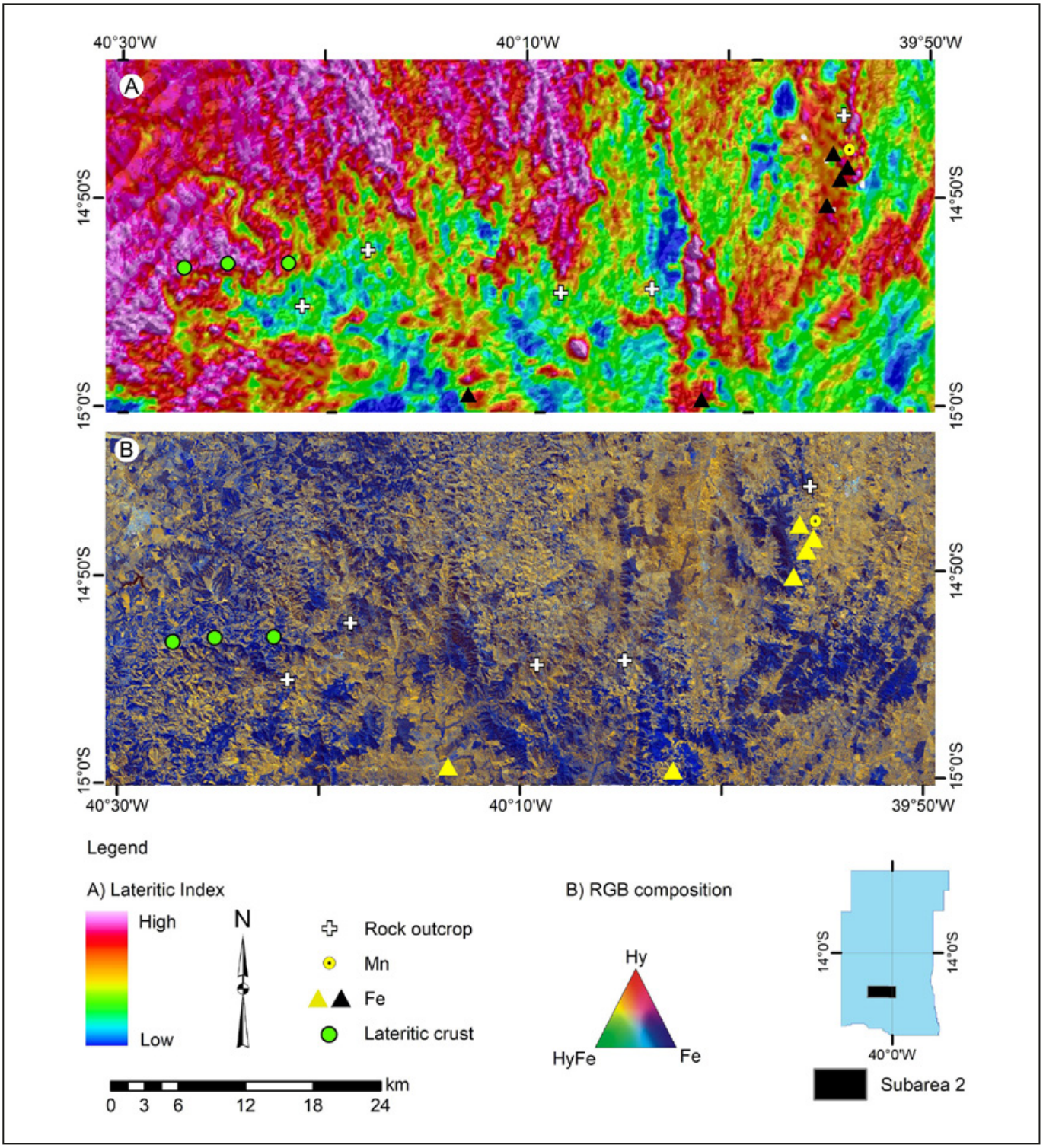

FIGURE 13 - A) Map of the lateritic index highlighting in magenta tones the most weathered areas and their occurrences of iron, manganese and ferruginous lateritic crusts. B) Color composition of images derived by Hy (R) -HyFe (G) -Fe (B) Crósta Technique, highlighting sectors with higher Fe (blue) presence, and dominated by hydroxyl- and iron-bearing minerals (yellow).

FIGURE 14 - A) Red soil with pink tones. B) Centimetric fragments of the aluminous crust.

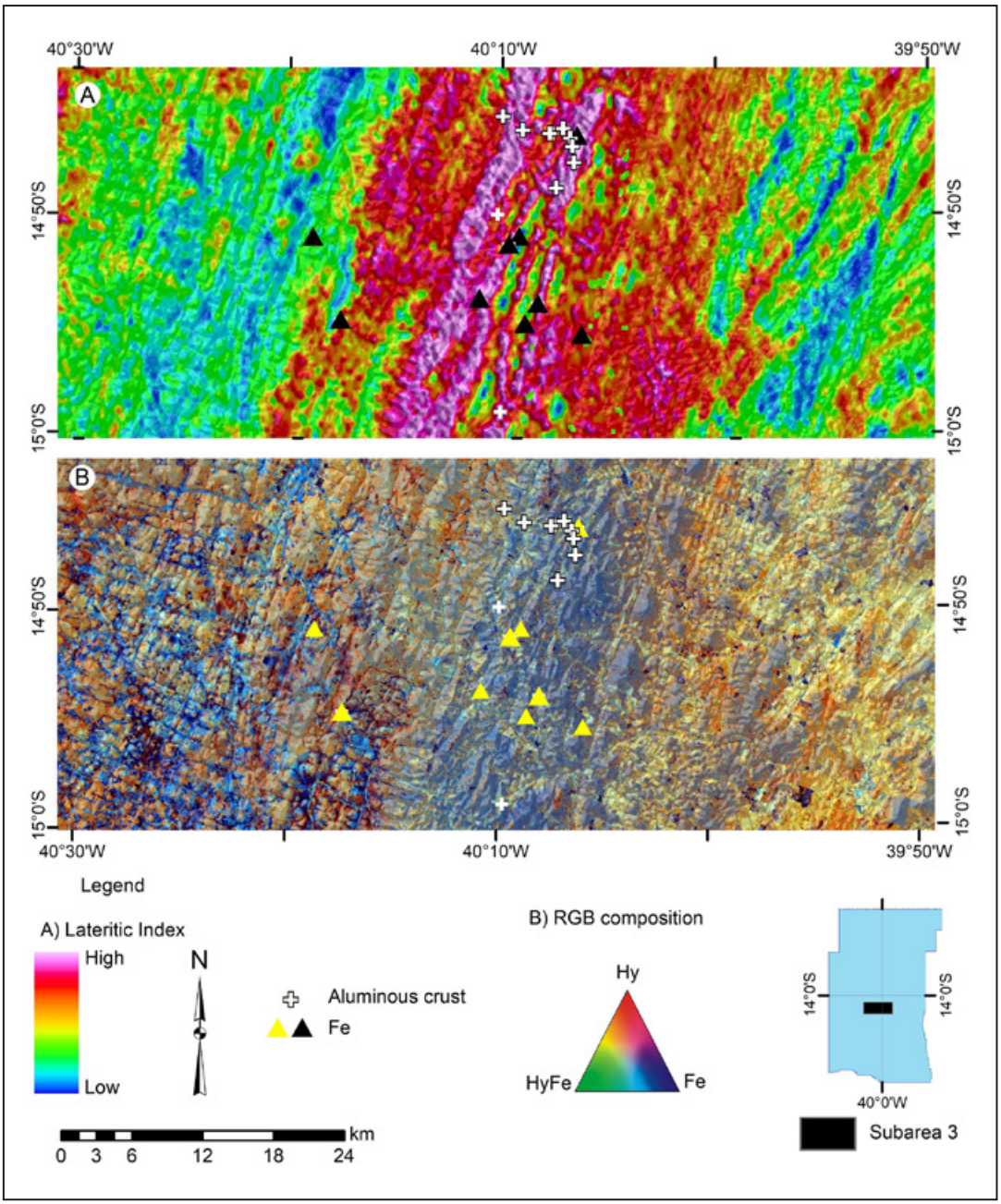

FIGURE 15 - A) Map of the lateritic index highlighting in magenta tones the most weathered areas and the occurrence of iron and alumina lateritic crusts. B) Color composition of images derived by Hy (R) -HyFe (G) -Fe (B) Crósta technique, highlighting sectors with higher Fe (blue) presence, and dominated by hydroxyl- and iron-bearing minerals carrier minerals.

interest. Thus, we suggest the development of the following future research activities:

1 Detailed study and mapping of lateritic profiles considering their maturity levels, horizons and geochemical associations;

2 Application of LI as additional information layer in prospective maps for Al, Fe, Mn, Ni, among others.

3 Mapping of the regolith in a pilot area, with the objective of improving and applying the procedures presented here, as well as pilot mapping of the regolith units of the region.

4 Use of machine learning algorithms (MLA) as neural networks and support vector machines to create more accurate predictive models for mineral prospecting using robust data from various sources.

Acknowledgements

The authors thank the Directory of Geology and Mineral Resources, the Division of Remote Sensing and Geophysics and the Management of Geology and Mineral Resources of the Superintendence of Salvador (SUREG-SA) of the Geological Service of Brazil that directly supported and encouraged this work. The authors also thank the two anonymous JGSB reviewers for their suggestions, which help us to improve the final version of the manuscript.

References

Albuquerque M.F.S. 2018. O contexto laterítico do sudeste do estado do Amazonas: uma abordagem mineralógica, geoquímica, aerogeofísica e eocronológica. PhD Thesis, Instituto de Geociências, Universidade de Brasília, Brasília, 167 p. Available on line at: http://repositorio.unb.br/handle/10482/32320

Almeida F.F.M., Hasui Y., Brito Neves B.B., Fuck R.A. 1981. Brazilian structural provinces: an introduction. Earth-Science Reviews, 17(1-2), 1-29. https://doi.org/10.1016/0012-8252(81)90003-9

Alves N.S. 2018. Petrografia e litogeoquímica do protominério de níquel laterítico de Calembe, Lajedo do Tabocal, Bahia. Graduation work, Universidade Federal da Bahia, Bahia, 112 p.

An P., Moon W.M., Rencz A. 1991. Application of fuzzy set theory to integrated mineral exploration. Canadian Journal of Exploration Geophysics, 27(1), 1-11.

Anand R.R., Butt C.R.M. 1988. The terminology and classification of the deeply weathered regolith. Australia, CSIRO Division of Exploration Geoscience. Discussion Paper.

Anand R.R., Smith R.E., Innes J., Churchward H.M., Perdrix J.L., Grunsky E.C. 1989. Laterite types and associated ferruginous materials, Yilgarn Block, WA: terminology, classification and atlas. Australia, CSIRO Division of Exploration Geoscience Report 60R.

Anand R.R., Paine M. 2002. Regolith geology of Yilgarn Craton, western Australia: implication for exploration. Australian Journal of Earth Sciences, 49, 3-162. https://doi.org/10.1046/j.1440-0952.2002.00912.x

Arhin E., Nude P.M. 2009. Significance of regolith mapping and its implication for gold exploration in northern Ghana: a case study at Tinga and Kunche. Geochemistry: Exploration, Environment Analysis, 9(1), 63-69. https://doi.org/10.1144/1467-7873/08-189

Arhin E., Jenkin G.R.T., Cunningham D., Nude O. 2015. Regolith mapping of deeply weathered terrain in savannah regions of the Birimian Lawra Greenstone Belt, Ghana. Journal of Geochemical Exploration, 159, 194-207. https://doi.org/10.1016/j.gexplo.2015.09.008

Batista J.A., Blanco J., Perez-Flores M.A. 2008. Geological interpretation of Eastern Cuba Laterites from an airborne magnetic and radioactive isotope survey. Geofísica Internacional, 47(2), 99-113.

Bonham-Carter G.F. 1994. Geographic information systems for geoscientists: modelling with GIS. Oxford, Pergamon Publications, 416 p. https://doi.org/10.1016/C2013-0-03864-9

Boissieu F., Sevin B., Cudahy T.,Mangeas M., Chevrel S., Ong C., Rodger A., Maurizot P., Laukamp C., Lau I., Touraivane T., Cluzel D., Despinoy M. 2018. Regolith-geology mapping with support vector machine: a case study over weathered Ni-bearing peridotites, New Caledonia. International Journal of Applied Earth Observation and Geoinformation, 64, 377-385. https://doi.org/10.1016/j.jag.2017.05.012

Briggs I.C. 1974. Machine Contouring Using Minimum Curvature. Geophysics, 39(1), 39-48. https://doi.org/10.1190/1.1440410

Butt C.R.M., Zeegers H. (ed.). 1992. Regolith Exploration Geochemistry in Tropical and Subtropical Terrains. Handbook of Exploration Geochemistry, 4. Elsevier, Amsterdam, p. 461-482.

Carranza E.J.M. 2009. Knowledge-driven modeling prospectivity. In: Carranza E.J.M. Geochemical anomaly and mineral prospectivity mapping in GIS. Amsterdam, Elsevier. p. 189-246. https://doi.org/10.1016/S1874-2734(09)70011-7

Carrino T.A., Silva A.M., Botelho N.F., Silva A.A.C. 2009. Detecção de ocorrências de coberturas supergênicas a partir de imagens altimétricas e gamaespectrométricas: os alvos do extremo leste do Amazonas. In: Simpósio Brasileiro de Sensoriamento Remoto, 14, 3197-3204.

Carrino T.A., Silva A.M., Botelho N.F., Silva A.A.C. 2011a. Discriminação de áreas de espesso regolito do leste do Estado do Amazonas usando estatística multivariada, algoritmo hiperespectral e modelagem de dados espaciais. Revista Brasileira de Geofísica, 29(1), 155-172. http://dx.doi.org/10.1590/S0102-261X2011000100011

Carrino T.A., Silva A.M., Botelho N.F., Silva A.A.C. 2011b. Análise prospectiva para ouro nas regiões de Ouro Roxo-Cantagalo e Chico Torres, província mineral do Tapajos. Revista Brasileira de Geofísica, 29(1), 135-154. http://dx.doi.org/10.1590/S0102-261X2011000100010

Companhia Baiana de Pesquisa Mineral (CBPM), Serviço Geológico do Brasil (CPRM). 2011. Projeto levantamento aerogeofísico da Área Ipirá-Ilhéus: relatório final de levantamento e processamento dos dados magnetométricos e gamaespectrométricos. Salvador, CBPM.

Companhia Baiana de Pesquisa Mineral (CBPM). 2007. Projeto levantamento aerogeofísico da área Ruy Barbosa / Vitória da Conquista: relatório final de aquisição e processamento de dados. Salvador, CBPM.

Companhia Baiana de Pesquisa Mineral (CBPM). 2009. Projeto levantamento aerogeofísico da área Cândido Sales / Mascote: relatório final de aquisição e processamento de dados. Salvador, CBPM.

Costa M.L. 1991. Aspectos geológicos dos lateritos da Amazônia. Belém, Revista Brasileira de Geociências, 21(2), 146-160.

Costa M.L 2007. Introdução ao intemperismo Laterítico e à Lateritização. In: Licht O.A.B., Mello C.S.B., Silva C.R. (ed.). Prospecção geoquímica de depósitos minerais metálicos, não Metálicos, óleo e gás. Rio de Janeiro, CPRM - Serviço Geológico do Brasil, 199-244.

Cohen J. 1960. A coefficient of agreement of nominal scales. Educational and Psychological Measurement, 20(1), 37-46. http://dx.doi.org/10.1177/001316446002000104.

Craig M.A., Anand R.R., Churchward H.M., Gozzard J.R., Smith R.E., Smith K. 1999. Regolith landform mapping in the Yilgarn Craton, Western Australia: towards a standardised approach. Wembley, CRC LEME.

Dauth C. 1997. Airborne magnetic, radiometric and satellite imagery for regolith mapping in the Yilgarn Craton of Western Australia. Exploration Geophysics 28(1-2), 199-203. https://doi.org/10.1071/EG997199

Dickson B.L., Scott K.M. 1997. Interpretation of aerial gamma-ray surveys - adding the geochemical factors. AGSO Journal of Australian Geology & Geophysics, 17(2), 187-200.

Eggleton R.A. (ed.). 2001. Glossary of regolith-surficial geology, soils and landscapes. Western Australia, CRC LEME, 144 p.

Fernandes P.C.D. 1995. Projeto terras raras no Complexo Jequié: relatório anual. Salvador, CPRM.

Freyssinet P.H., Butt C.R.M., Morris R.C., Piantone P. 2005. Ore-forming processes related to lateritic weathering. In: Hedenquist J.W., Thompson J.F.H., Goldfarb R.J., Richards J.P. Economic geology: one hundredth anniversary volume. Colorado, Society of Economic Geologists, p. 681-722. https://doi.org/10.5382/AV100.21

Herrera I.L.I.E. 2016. Utilização de dados altimétricos, geomorfológicos e gamaespectrométricos para a identificação de crostas lateríticas em uma área da porção norte do estado de Rondônia. MSc Dissertation, Universidade Federal de Rondônia, Porto Velho.

Herrera I.L.I.E., Silva Filho E.P., Iza E.R.H.F., Horbe A.M.C. 2016. Cartografia geológica e geomorfológica de crostas lateríticas na porção norte do estado de Rondônia. Revista Brasileira de Geomorfologia, 17(1), 177-190. http://dx.doi.org/10.20502/rbg.v17i1.880

Iza E.R.H.F., Horbe A.M.C, Silva A.M. 2016a. Boolean and fuzzy methods

for identifying lateritic regoliths in the Brazilian Amazon using gamma-ray spectrometric and topographic data. Geoderma, 269, 27-38. https://doi.org/10.1016/j.geoderma.2016.01.037

Iza E.R.H.F., Horbe A.M.C., Herrera I.L.I.E. 2016b. Use of gamma spectrometric and altimetric data to map lateritic crusts on the Western portion of the Brazilian Amazon. In: Simpósio Brasileiro de Exploração Mineral, 7.

Iza E.R.H.F. 2017. Coberturas lateríticas do SW do Cráton Amazônico: aspectos geofísicos e geoquímicos. PhD Thesis, Instituto de Geociências, Universidade de Brasília, Brasília, 73 p.

Iza E.R.H.F., Horbe A.M.C., Castro C.C., Herrera I.L.I.E. 2018. Integration of geochemical and geophysical data to characterize and map lateritic regolith: an example in the Brazilian Amazon. Geoquemistry, Geophysics, Geosystems, 19(9), 3254-3271. https://doi.org/10.1029/2017GC007352

Iza E.R.H.F., Santos R.S.V., Cruz Filho B.E. 2019a. Mapa de correlação entre o índice laterítico e o gradiente total [do leste do Cráton São Francisco], Escala1:750.000. Salvador, CPRM. Available on line at: http://rigeo.cprm.gov.br/jspui/bitstream/doc/21181/1/correlacao_indice_gradiente.pdf

Iza E.R.H.F., Santos R.S.V., Cruz Filho B.E. 2019b. Mapa do índice laterítico [do Leste do Cráton São Francisco], Escala 1:750.000. Salvador, CPRM. Available on line at: http://rigeo.cprm.gov.br/jspui/bitstream/doc/21183/1/indice_lateritico.pdf

Kearey P., Broooks M., Hill I. 2002. An introduction to geophysical exploration. Oxford, Blackwell Science, 262 p. https://doi.org/10.1046/j.1365-246X.2003.01868.x

King L.C. 1956. A geomorfologia do Brasil Oriental. Revista Brasileira de Geografia, 18(2), 147-266.

Lagacherie P. 2005. An algorithm for fuzzy pattern matching to allocate soil individuals to preexisting soil classes. Geoderma, 128(3-4), 274-288. https://doi.org/10.1016/j.geoderma.2005.04.009

Landis J.R., Koch G.G. 1977. The measurement of observer agreement for categorical data. Biometrics, 33(1), 159-174. http://dx.doi.org/10.2307/2529310

Loughlin W. 1991. Principal component analysis for alteration mapping. Photogrammetric Engineering and Remote Sensing, 57, 1163-9.

Martins A.A.M., Santos R.A. (org.). 1997. Ibicaraí, folha SD.24-Y-B-V: estado da Bahia, escala 1:100.000. Brasília, CPRM. 237 p.

McBratney A.B., Mendonça Santos M.L., Minasny B. 2003. On digital soil mapping. Geoderma, 117(2), 3-52. https://doi.org/10.1016/S0016-7061(03)00223-4

McQueen K.G., Craig M.A. 1995. Developments and new approaches in regolith mapping. Canberra, Centre for Australian Regolith Studies, 86 p.

Moreira F.R.S., Almeida-Filho R., Camara G. 2003. Spatial analysis techniques applied to mineral prospecting: an evaluation in the Poços de Caldas Plateau. Revista Brasileira de Geociências, 33(2), 183-190. https://doi.org/10.25249/0375-7536.200333S2183190

Minty B.R.S. 1997. Fundamentals of airborne gamma-ray spectrometry. AGSO Journal of Australian Geology and Geophysics, 17, 39-50.

Minty B. 2011. Short note: on the use of radioelement ratios to enhance gamma-ray spectrometric data. Exploration Geophysics, 42(1), 116-120. https://doi.org/10.1071/EG10011

NASA. Shuttle Radar Topography Mission-SRTM. Available on line at: http://www2.jpl.nasa.gov/srtm/index.html / (accessed on: 28 February 2019)

Pedreira A.J., Arcanjo J.B., Pedrosa C.J., Oliveira J.E., Silva B.C.E., Mascarenhas J.F. 1975. Projeto Bahia: relatório final. Geologia da Chapada Diamantina. Salvador, CPRM.

Santos C.B. 2010. Avaliação hidrogeológica do alto da Bacia do Rio Jiquiriçá, Estado da Bahia. PhD Thesis, Universidade Federal da Bahia, Salvador, 190 p.

Scott K.M., Pain C.F. 2008. Introduction. In: Scott K.M., Pain C.F. (ed.). Regolith Science. Dordrecht, Springer Science, p. 1-6.

Silva Filho M.A., Moraes Filho O., Gil C.A.C., Santos R.A. 1974. Projeto sul da Bahia: relatório final. Salvador, DNPM/CPRM, v. 15.

Silva R.W.S., Sampaio E.E.S. 2017. Geofísica na Bahia: estudos geológicos e exploração mineral. Salvador, CBPM, 648 p.

Souza J.D.M, Campelo R., Kosin M. 2003. Mapa geológico do estado da Bahia, Escala 1:1.000.000. Salvador, CPRM. Available on line at: http://rigeo.cprm.gov.br/jspui/handle/doc/8665

Smith R.E., Anand A.R.R., Alley N.F. 2000. Use and implications of paleoweathering surfaces in mineral exploration in Australia. Ore Geology Reviews, 16(3-4), 185-204. https://doi.org/10.1016/S0169-1368(99)00030-X

Takeno N. 2005. Atlas of Eh-pH diagrams: intercomparison of thermodynamic databases. Japão, National Institute of Advanced Industrial Science and Technology, 287 p. Available on line at: https://www.gsj.jp/researches/openfile/ openfile2005/openfile0419.html / (accessed on: 15 February 2019)

Thomas M.F. 1974. Tropical geomorphology: a study of weathering and landform development in warm climates. New York, John Wiley & Sons, 332 p.

United States Geological Survey (USGS). 2019. Available on line at: http://glovis.usgs.gov / (Accessed on: 15 February 2019)

Wedepohl K.H. 1969. Handbook of geochemistry. New York, Springer-Verlag, 578 p.

Wilford J.R. 1992. Regolith mapping using integrated Landsat TM imagery and high resolution gamma-ray spectrometric imagery: Cape York Peninsula. Canerra City, Australian Geological Survey Organisation, 41 p.

Wilford J.R., Bierwirth P.N., Craig M.A. 1997. Application of airborne gamma-ray spectrometry in soil/regolith mapping and applied geomorphology. Journal of Australian Geology & Geophysics, 17(2), 201-216.

Wilford J.R. 2002. Airborne Gamma-Ray Spectrometry. In: Papp E. (ed.). Geophysical and remote sensing methods for regolith exploration. Australia, CRCLEME, 46-52.

Wilford J.R. 2012. A weathering intensity index for the Australian continent using airborne gamma-ray spectrometry and digital terrain analysis. Geoderma, 183-184, 124-142. https://doi.org/10.1016/j.geoderma.2010.12.022

Wilford J.R. 2013. New regolith mapping aproaches for old australian landscapes. PhD Thesis, School of Earth and Environmental Sciences, University of Adelaide, 183 p.

Zimmermann H.J. 1985. Fuzzy set theory and its applications. Boston, Springer Netherlands, 363 p. https://doi.org/10.1007/978-94-015-7153-1